nature medicine

Article

https://doi.org/10.1038/s41591-025-03704-9

Lutetium-177–PSMA-617 or cabazitaxel in metastatic prostate cancer: circulating tumor DNA analysis of the randomized phase 2 TheraP trial

Received: 5 November 2024

Accepted: 7 April 2025

Published online: 27 May 2025

Check for updates

A list of authors and their affiliations appears at the end of the paper

The prostate-specific membrane antigen (PSMA)-targeted radioligand [^{177}Lu]Lu–PSMA-617 is a new standard treatment for metastatic castration-resistant prostate cancer (mCRPC), but predictive genomic biomarkers informing its rational use are unknown. We performed detailed dissection of prostate cancer driver genes across 290 serial plasma cell-free DNA samples from 180 molecular imaging-selected patients with mCRPC from the randomized TheraP trial of [^{177}Lu]Lu–PSMA-617 (n = 97) versus cabazitaxel chemotherapy (n = 83). The primary endpoint was PSA50 biochemical response, with secondary endpoints of progression-free survival (PFS) and overall survival (OS). In this post-hoc biomarker analysis, a low pretreatment circulating tumor DNA (ctDNA) fraction predicted a superior biochemical response (100% versus 58%, P = 0.0067) and PFS (median 14.7 versus 6.0 months; hazard ratio 0.12, $P = 2.5 \times 10^{-4}$) on [^{177}Lu]Lu–PSMA-617 independent of predictive PSMA–positron emission tomography imaging parameters, although this benefit did not extend to OS. Deleterious *PTEN* alterations were associated with worse PFS and OS on cabazitaxel, whereas *ATM* defects were observed in select patients with favorable [^{177}Lu]Lu–PSMA-617 outcomes. Comparing pretreatment and progression ctDNA revealed population flux but no evidence that alterations in individual mCRPC genes (or *FOLH1*) are dominant causes of acquired [^{177}Lu]Lu–PSMA-617 or cabazitaxel resistance. Our results nominate new candidate biomarkers for [^{177}Lu]Lu–PSMA-617 selection and ultimately expand the mCRPC predictive biomarker repertoire. We anticipate our ctDNA fraction-aware analytical framework will aid future precision management strategies for [^{177}Lu]Lu–PSMA-617 and other PSMA-targeted therapeutics. ClinicalTrials.gov identifier: NCT03392428.

e-mail: ian.davis@monash.edu; michael.hofman@petermac.org; arun.azad@petermac.org; alexander.wyatt@ubc.ca

Prostate-specific membrane antigen (PSMA)-targeted radioligand therapy is the most promising new therapy class in advanced prostate cancer, spurred by the approval of lutetium-177 [^{177}Lu]Lu–PSMA-617 (LuPSMA) for PSMA-positive metastatic castration-resistant prostate cancer (mCRPC). We previously reported results from TheraP, a randomized phase 2 trial comparing LuPSMA with cabazitaxel in progressive mCRPC following docetaxel chemotherapy[1,2]. LuPSMA achieved significantly higher biochemical and objective response rates, longer progression-free survival (PFS) and improved quality of life[1], with similar overall survival (OS) outcomes to cabazitaxel[2]. The phase 3 registrational VISION study of LuPSMA plus standard-of-care versus standard-of-care alone in mCRPC demonstrated superior outcomes for LuPSMA[3]. Expansion of approved indications is likely as PSMA radioligand therapy continues to be tested in early- and late-stage prostate cancer, both as monotherapy and in combination. There is a pressing need to develop personalized strategies based on contemporaneous disease to rationalize selection of LuPSMA versus other life-prolonging systemic therapies.

Molecular imaging provides real-time insights into disease biology and shows potential for enhancing outcome stratification in patients receiving LuPSMA[4]. Prespecified analysis in TheraP and exploratory analysis in VISION corroborated high PSMA tumor uptake (mean standardized uptake value (SUVmean) ≥10) to enrich for deep and durable LuPSMA responses[5,6]. Metabolic tumor volume (MTV) as measured by 2-[^{18}F]fluoro-2-deoxy-D-glucose (FDG) positron emission tomography (PET) is strongly prognostic for OS in patients treated with cabazitaxel or LuPSMA[2,5]. Furthermore, a subset of patients with low PSMA uptake and/or 2-[^{18}F]FDG-discordant disease experience disproportionately poor outcomes[2,7], and were excluded from the TheraP study. Collectively, these imaging features form the foundation for developing a biomarker-informed treatment selection framework in patients potentially suitable for LuPSMA.

Genomic alterations guide targeted treatment selection in multiple solid cancers. In mCRPC, alterations in DNA repair genes inform use of poly(ADP-ribose) polymerase inhibitors (PARPi)[8] and immune checkpoint inhibitors[9]. Genomic testing in mCRPC traditionally relied upon archival primary tumor tissue specimens[10], but plasma cell-free circulating tumor DNA (ctDNA) profiling has emerged as a practical means to identify current alterations, including those associated with treatment resistance[11,12]. To date, there are no ctDNA- or tissue-based biomarkers influencing the use of LuPSMA or taxane chemotherapy, although retrospective cohort studies have nominated ctDNA features linked to LuPSMA outcomes[13–17]. However, without a comparator arm, these studies could not resolve predictive from prognostic features. To address this unmet need, we performed an exploratory correlative analysis of ctDNA features from baseline and progression samples from the randomized TheraP trial.

Results

Study cohort

TheraP (ANZUP 1603; NCT03392428) was an open-label, phase 2 trial that randomized 200 individuals with progressive mCRPC following prior docetaxel to receive LuPSMA or cabazitaxel[1,2]. A total of 91% of participants previously received androgen receptor pathway inhibitors (ARPI) abiraterone and/or enzalutamide (16% received both). Participants were screened with [^{68}Ga]Ga–PSMA-11 (PSMA-PET) and 2-[^{18}F]FDG-PET (FDG-PET) to select for high PSMA uptake at metastatic site(s) without discordant disease (2-[^{18}F]FDG-positive lesion with low or no PSMA uptake)—distinct from trials using PSMA-PET-only eligibility assessment[3,18,19]. Further details are described in the Methods and previous publications[1,2,5].

In total, 183 patients received at least one dose of LuPSMA or cabazitaxel. Blood samples were collected before treatment in 98% (180 of 183) of patients (Fig. 1a and Extended Data Fig. 1). Patient characteristics and treatment efficacy were similar in participants with pretreatment samples (n = 180) and the overall population (n = 200) (Supplementary Table 1). Median baseline cell-free DNA (cfDNA) concentration and total yield were 13 ng ml^{-1} plasma (interquartile range (IQR) 8.0–41) and 66 ng (IQR 38–199), respectively (Supplementary Table 2). cfDNA underwent deep targeted sequencing using a validated custom prostate cancer research assay[20,21], enabling allele-specific resolution of somatic mutations, chromosomal aneuploidies, focal copy number alterations and complex structural rearrangements. Synchronous sequencing of matched white blood cell (WBC) DNA allowed discrimination of tumor-specific from germline and clonal hematopoiesis variants. Two baseline cfDNA samples failed sequencing and were excluded from analyses—the remaining 178 samples formed the biomarker population (Extended Data Fig. 1). WBC DNA was unavailable in four patients. Sixty percent (106 of 178) of participants had both baseline and progression blood samples to investigate temporal clonal dynamics and acquired resistance (Fig. 1a). All WBC DNA and progression cfDNA was successfully sequenced (Supplementary Table 2).

ctDNA fraction (ctDNA%) is an established independent prognostic factor across multiple disease and treatment contexts, serving as a proxy for metastatic disease burden and cancer aggression[20–22]. We measured ctDNA% via genome-wide aneuploidy and somatic mutations (enabling orthogonal validation) using published benchmarked methodology (Supplementary Table 3)[12,23]. For outcomes analysis, participants were stratified into predefined prognostic categories of low or undetected (<2%), medium (2–30%) and high ctDNA% (>30%) as previously described[20,24]. Baseline ctDNA% was similar between treatment arms (P = 0.95, Mann–Whitney U-test) (Fig. 1b). Consistent with a heavily pretreated mCRPC population, median baseline ctDNA% was 28% (IQR: 15–51%, range: 2.1–83%) among the 150 (85%) patients with ctDNA ≥2%—higher than previous trials in ARPI- and/or taxane-naive first-line mCRPC (median ctDNA: 17%)[24] but similar to clinical poor-risk disease (median ctDNA: 24%)[25]. In the TheraP biomarker population (n = 178), higher ctDNA% was expectedly correlated with hematologic and biochemical prognostic markers (Fig. 1c) and attenuated PFS and OS (Fig. 1d).

Pretreatment ctDNA fraction predicts differential outcomes

Whole-body quantitative PSMA-PET and FDG-PET parameters can risk-stratify mCRPC receiving LuPSMA[2,5,26], but no prostate cancer studies have compared molecular imaging features and ctDNA%. To assess the independent biomarker potential of baseline ctDNA% and explore opportunities for integrating with molecular imaging, we first defined the relationship between synchronous ctDNA% and PET imaging parameters. Most volumetric and avidity parameters were co-correlated with ctDNA% (Fig. 1e). Baseline ctDNA% was moderately positively correlated with whole-body PSMA total tumor volume (R = 0.51, $P = 7.3 \times 10^{-12}$) and FDG MTV (R = 0.57, $P = 1.6 \times 10^{-15}$) (Fig. 1e and Extended Data Fig. 2). Patients with high ctDNA% (>30%) had lower median PSMA SUVmean (8.0 versus 10.6 in patients with ctDNA <2%, $P = 1.24 \times 10^{-4}$, Mann–Whitney U-test) and were less frequently observed to have PSMA SUVmean ≥10 (16% versus 61%, Fisher's exact test), the latter shown in a prespecified analysis to be predictive for prostate-specific antigen (PSA) response and prognostic for OS (Fig. 1f and Supplementary Table 4)[2,5]. High ctDNA% was also strongly linked to a higher likelihood of 2-[^{18}F]FDG MTV ≥ 200 ml, which is prognostic for PSA response and OS on both LuPSMA and cabazitaxel (Fig. 1f and Supplementary Table 4)[2,5].

The potential for baseline ctDNA% to inform selection between LuPSMA and another active standard-of-care therapy such as cabazitaxel is incompletely understood. Individuals with low ctDNA% (<2%; representing 16% of biomarker population) had a significantly higher PSA50 response rates (PSA reduction of ≥50% from baseline) on LuPSMA compared with cabazitaxel (16 of 16 (100%) versus 7 of 12 (58%); odds ratio (OR) infinite, P = 0.0067) (Fig. 2a). This difference in PSA50 response between treatment arms diminished at higher

ctDNA% categories, only modestly favoring LuPSMA for medium ctDNA% (OR = 3.2 for 2–30% ctDNA, $P = 0.015$), with no difference for high ctDNA% (>30%). The differential PSA50 response between treatment arms, as influenced by ctDNA%, remained significant when ctDNA% was analyzed as a continuous variable (interaction $P = 0.047$).

Baseline ctDNA% provided significantly greater stratification of PFS for LuPSMA compared with cabazitaxel (Fig. 2b; interaction $P = 0.032$). This was primarily attributed to patients with low ctDNA% disproportionately benefiting from LuPSMA over cabazitaxel, with an 8.7 month increase in median PFS (14.7 versus 6.0 months, $P = 2.5 \times 10^{-4}$), exceeding the overall benefit of LuPSMA in the biomarker-unselected population (Fig. 2b; HR = 0.12 versus 0.63, interaction $P = 0.014$). High ctDNA% was conversely associated with outcomes comparable with both LuPSMA and cabazitaxel (median PFS 3.0 and 2.8 months for LuPSMA and cabazitaxel, respectively; HR = 1.1, $P = 0.79$). Among patients with low ctDNA%, baseline PSMA SUVmean was significantly higher in the LuPSMA arm than in the cabazitaxel arm (median 12 versus 9, $P = 0.017$). Nevertheless, low ctDNA% remained independently predictive for superior PFS on LuPSMA versus cabazitaxel in a multivariable analysis incorporating baseline PSMA SUVmean, the only established predictive response biomarker for LuPSMA (multivariable HR = 0.34, $P = 0.029$ when dichotomized at 10 (Fig. 2b); multivariable HR = 0.31, $P = 0.017$ as a continuous variable). Consistent with PSMA-PET and ctDNA% each offering an independent predictive value, combining both parameters further stratified outcomes in patients with both high and low PSMA SUVmean receiving LuPSMA, caveated by relatively small subgroups (Fig. 2c). Baseline ctDNA% was strongly prognostic in the overall biomarker population (Fig. 1d) although not predictive for OS (interaction $P = 0.67$) across any baseline ctDNA% risk category (Fig. 2d). Collectively, these data suggest that ctDNA% is a candidate predictive and prognostic biomarker for differential response to LuPSMA versus cabazitaxel chemotherapy in patients with molecular imaging-selected mCRPC progressing after docetaxel.

ctDNA-derived features of molecular imaging-selected mCRPC

Next, we defined the frequency of genomic driver alterations in evaluable baseline ctDNA samples (Methods). For select clinically relevant prostate cancer genes, we additionally inferred the number of disrupted versus functionally intact alleles by enumerating all independent single-allele defects (mutations, intragenic deletions, structural variants) on a scaffold of local ploidy (Fig. 3a, Methods and Supplementary Table 5). Our assay captured both exons and select introns, enabling characterization of focal intragenic copy alterations and structural variants with intronic breakpoints—alteration classes with established relevance in mCRPC from whole-genome sequencing studies[12,27].

The most frequently altered genes were *AR* (68%), *TP53* (53%) and *PTEN* (35%) (Fig. 3b–d). Gene-disrupting structural variants were a substantial mechanism of inactivation in *TP53*, *PTEN* and *BRCA2* (Fig. 3b and Extended Data Fig. 3). Notably, disruption of all *TP53* and *PTEN* alleles resulting in null status (all copies disrupted, Methods) was observed in 37% and 23% of participants with ctDNA ≥2%, respectively (Fig. 3b). Mutational frequencies were consistent with previous ctDNA and metastatic tissue studies in unselected first- and/or second-line mCRPC[23,24,28], despite the dual-tracer imaging selection in TheraP (Fig. 3c). Consistent with near-ubiquitous exposure to ARPIs, the *AR* gene and enhancer locus were perturbed by combinatorial mechanisms including copy gain (≥4 absolute copies; 50% (*AR* gene), 60% (*AR* enhancer) in patients with ctDNA ≥5%), ligand-binding domain (LBD) mutations (18%), and structural rearrangements predicted to truncate the LBD (23%) (Fig. 3d). Expectedly, LBD mutations were enriched in samples without *AR* gain (68% versus 32%; $P = 0.049$, Fisher's exact test), whereas LBD-truncating rearrangements were more common in samples with *AR* amplification (37% in ≥8 copies versus 19% in <8 copies; $P = 0.025$, Fisher's exact test)[23,24]. *AR* gene and enhancer copy number were highly correlated (Pearson's $r = 0.77$; $P = 2.3 \times 10^{-28}$). In total, 46 of 150 (31%) patients with ctDNA ≥2% harbored deleterious germline and/or somatic alterations in ≥1 DNA damage repair (DDR) gene, most commonly in *BRCA2* (7%), *ATM* (7%) and *CDK12* (7%)—*CDK12* and *ATM* were mostly mutually exclusive with *TP53* alterations (Fig. 3e). Fifty-nine percent of evaluable samples showed evidence of whole-genome duplication (WGD). Alteration frequency was balanced across treatment arms (Supplementary Table 6).

Next, we intersected PSMA SUVmean and FDG MTV with the most prevalent genotypes. *PTEN* alterations were linked to a 14% reduction in PSMA SUVmean expression ($P = 0.026$, Mann–Whitney *U*-test), but a 95% increase in FDG MTV ($P = 0.0062$, Mann–Whitney *U*-test) (Fig. 3f and Extended Data Fig. 4), the latter compatible with phosphatidylinositol-3-kinase (PI3K) pathway upregulation mediating increased glycolysis[29]. These associations persisted after accounting for the strong effect of ctDNA% on both parameters (Fig. 1f). We observed no association between PSMA SUVmean and alteration status in *TP53*, *AR* or other common driver alterations (Fig. 3f–h).

Biomarker utility of baseline genomic alterations

Genomic alterations in ctDNA are linked to outcomes in early mCRPC treated with ARPI[24,25,30–33]. To explore these associations in the clinically advanced TheraP population (both treatment arms combined), we intersected clinical outcomes with baseline genomic features among three most frequently altered driver genes: *TP53*, *AR* and *PTEN*, while separately stratifying individuals with ctDNA <2% in whom somatic alteration status was not derived. *TP53* alterations were associated with significantly worse PFS and OS, whereas neither *PTEN* nor *AR* alterations were strongly prognostic in the ctDNA ≥2% population (Extended Data Figs. 5 and 6), contrasting earlier studies investigating ARPI outcomes in early mCRPC[24,25,30–33]. Supplementary Table 7 summarizes the prognostic relevance of less frequently altered genes.

Across clinical subgroups, neither treatment demonstrated a distinct advantage for PSA50 response, PFS or OS, consistent with the overall biomarker population in which LuPSMA generally showed better outcomes except for OS (Extended Data Fig. 7). Next, we used a gated two-tiered hypothesis testing strategy to understand whether selected high-prevalence (≥10%) genomic alterations predict differential treatment outcomes: first testing binary alteration presence or absence (any pathogenic alteration; excluding monoallelic deletions), then stratifying by compound alteration status (Methods and Supplementary Table 5). To address the confounder of ctDNA% (Figs. 1d

Fig. 1 | Study design and baseline clinical genomic correlates. a, Overview of sample collection and ctDNA genomic correlative analysis strategy in the TheraP study. **b**, Distribution of targeted sequencing-derived ctDNA% in baseline and progression cfDNA samples stratified by treatment arm and compared with published cohorts[24,25]. **c**, Distribution of routine prognostic laboratory values stratified by ctDNA% categories of <2%, 2–30% and >30%. Baseline lactate dehydrogenase data were available in 91 of 178 (51%) patients with baseline cfDNA; all other laboratory values were available in full. **d**, Kaplan–Meier estimates of PFS and OS stratified by baseline ctDNA%. In-set tables show univariable HR from a Cox proportional hazards model. **e**, Correlation matrix showing relationship between ctDNA% (continuous variable) and quantitative PSMA-PET and FDG-PET imaging parameters. Spearman's rho is annotated. Asterisks indicate correlations between variables with *P* values <0.05, adjusted for multiple hypothesis testing using the Bonferroni correction ($\alpha = 0.05$, $m = 21$ hypotheses). **f**, Distribution of PSMA SUVmean and FDG MTV stratified by baseline ctDNA% category. Horizontal dashed lines represent previously established clinically relevant thresholds for high PSMA expression (SUVmean ≥10) and high FDG MTV (≥200 ml)[5]. *P* values reflect two-sided Mann–Whitney *U*-tests adjusted for multiple hypothesis testing using the Bonferroni correction ($\alpha = 0.05$, $m = 3$ hypotheses). C, cycle; MAF, mean allele fraction; mPFS, median progression-free survival; mOS, median overall survival; NR, not reached; Ref, reference; TTV, total tumor volume; Tx, treatment.

https://doi.org/10.1038/s41591-025-03704-9

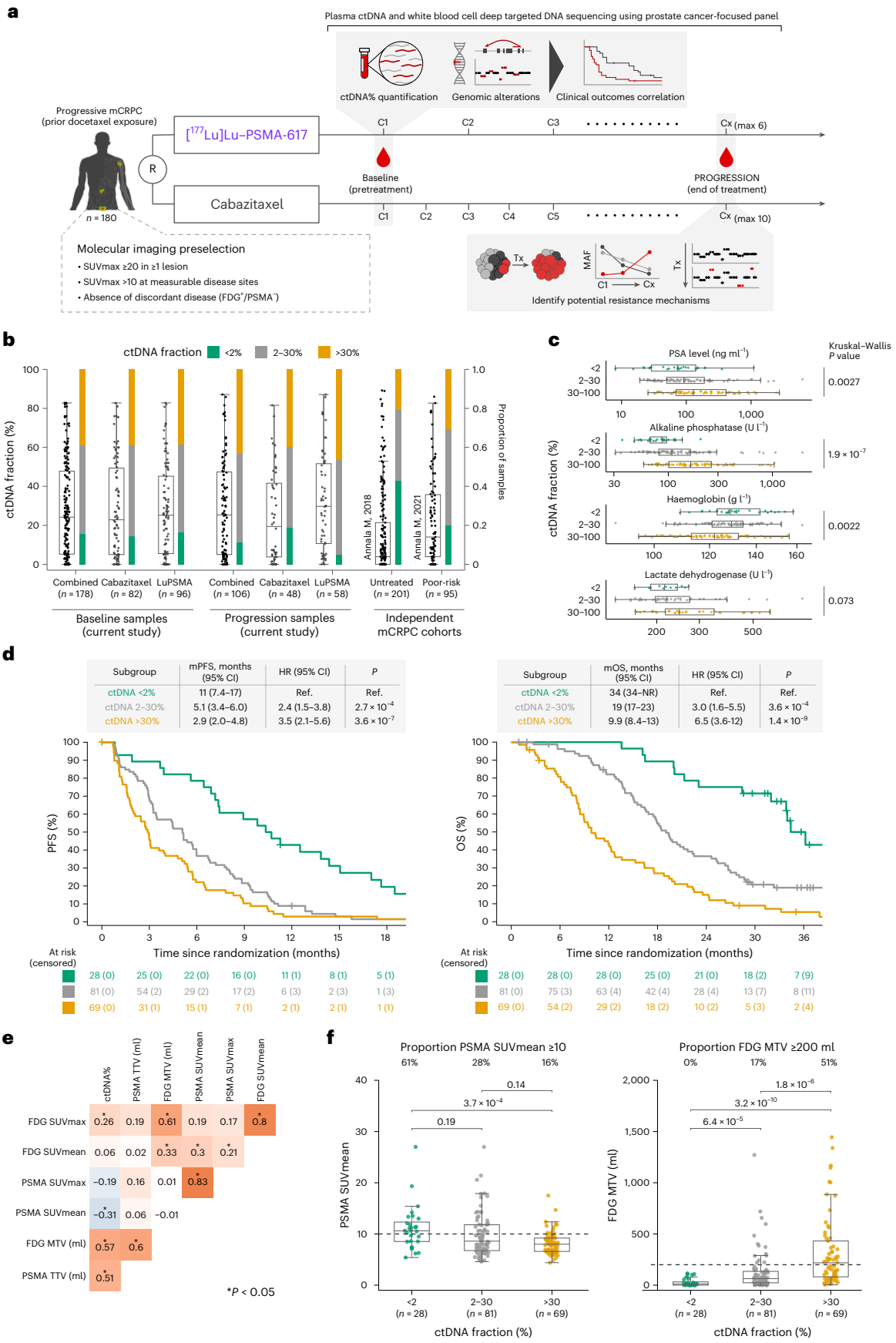

https://doi.org/10.1038/s41591-025-03704-9

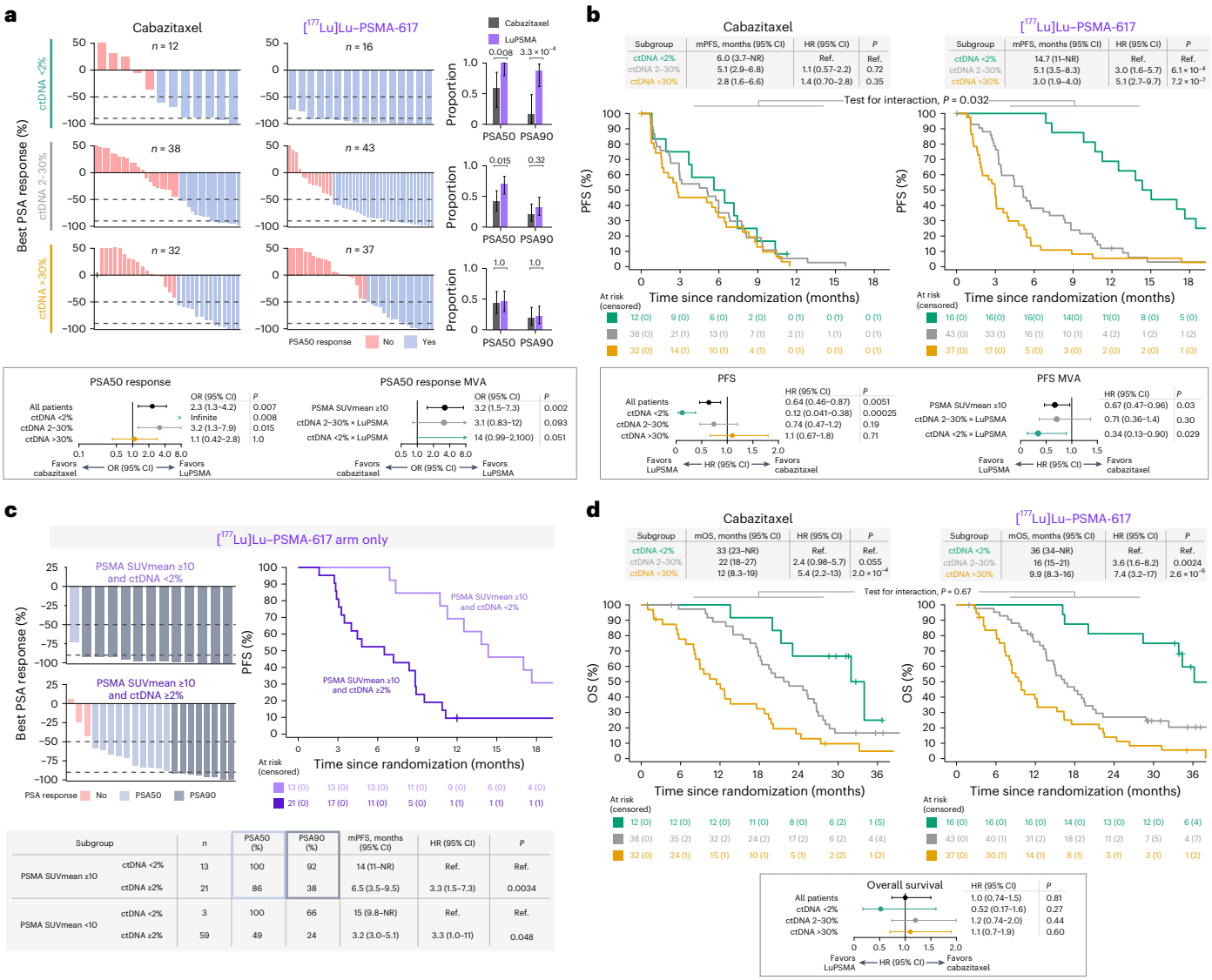

Subgroup		n	PSA50 (%)	PSA90 (%)	mPFS, months (95% CI)	HR (95% CI)	P
PSMA SUVmean ≥10	ctDNA <2%	13	100	92	14 (11–NR)	Ref.	Ref.
	ctDNA ≥2%	21	86	38	6.5 (3.5–9.5)	3.3 (1.5–7.3)	0.0034
PSMA SUVmean <10	ctDNA <2%	3	100	66	15 (9.8–NR)	Ref.	Ref.
	ctDNA ≥2%	59	49	24	3.2 (3.0–5.1)	3.3 (1.0–11)	0.048

Fig. 2 | Clinical outcomes by pretreatment ctDNA%. a, Waterfall plots of best PSA response stratified by baseline ctDNA category for patients allocated to cabazitaxel or LuPSMA (mCRPC). Summary bar plots (right) represent the proportion of patients who experienced a PSA50 and PSA90 response, stratified by treatment arm. Error bars denote the Clopper–Pearson exact 95% CI for binomial proportions. *P* values reflect two-sided Fisher's exact tests comparing the proportion of patients achieving each type of PSA response across ctDNA% categories. Forest plots show post-hoc sensitivity analyses for PSA50 and PSA90 responses according to ctDNA% category. Here and in the PFS forest plot in **b**, the 'All patients' category represents the entire biomarker population with baseline cfDNA passing quality control ($n = 178$). **b**, Kaplan–Meier estimates of PFS stratified by baseline ctDNA% categories in the biomarker-evaluable population ($n = 178$ total; $n = 82$ and $n = 96$ randomized to cabazitaxel and LuPSMA, respectively). In-set tables show univariable HR from a Cox proportional hazards model. The left-most forest plot shows post-hoc sensitivity analyses for PFS according to ctDNA% categories. The right-most forest plot shows an interaction test between treatment arm (reference category cabazitaxel arm) and ctDNA% category (reference category ctDNA >30%) in the entire biomarker population ($n = 178$), with an additional covariate of PSMA SUVmean (dichotomized at ≥10 or <10). **c**, Top, waterfall plots of best PSA response and Kaplan–Meier estimates of PFS in participants receiving LuPSMA with PSMA SUVmean ≥10 stratified by ctDNA% (<2% versus ≥2%). Bottom, in-set table shows PSA response percentage and univariable HR from a Cox proportional hazards model by PSMA SUVmean (≥10 and <10) and ctDNA% (<2% and ≥2%). **d**, Kaplan–Meier estimates of OS stratified by baseline ctDNA% category in the biomarker-evaluable population ($n = 178$ total; $n = 82$ and $n = 96$ randomized to cabazitaxel and LuPSMA, respectively). In-set tables show univariable HR from a Cox proportional hazards model. All forest plots (**a**, **b** and **d**) show HR and 95% CI.

and 2 and Extended Data Figs. 3 and 4), we focused on patients with ≥2% ctDNA, and adjusted for ctDNA% as a continuous covariate in multivariable analyses.

PTEN alterations were associated with a higher PSA50 response rate (58% versus 33%; OR = 2.8, $P = 0.097$) and modest PFS improvement on LuPSMA versus cabazitaxel (cross-arm comparison, median 3.4 versus 1.7 months; HR = 0.55, $P = 0.049$) (Fig. 4a and Supplementary Table 8), with an interaction test *P* value of 0.092 between treatment arm and *PTEN* status in individuals with detected ctDNA (Fig. 4b). This difference among participants with altered *PTEN* was driven by poor outcomes on cabazitaxel (per-arm comparison: HR = 2.0 for *PTEN*-altered among patients with ctDNA ≥2%, $P = 0.016$), whereas LuPSMA outcomes did not differ by *PTEN* status (per-arm comparison: HR = 1.1 for *PTEN*-altered among patients with ctDNA ≥2%, $P = 0.82$) (Fig. 4b,c and Supplementary Table 9). Importantly, the relationship between *PTEN* status and PFS was consistent across *PTEN* alteration subgroups (for example, total allelic inactivation versus any alteration) and mirrored when analyzing OS: patients with altered *PTEN* receiving LuPSMA had a 6.1-month improvement in median OS relative to cabazitaxel (HR = 0.39, $P = 0.022$) (Fig. 4b and Supplementary Table 8).

The positive interaction between treatment and *PTEN* status for OS was preserved after adjusting for ctDNA% (continuous covariate) and PSMA SUVmean ≥10 (Fig. 4b). Taken together, these results suggest that LuPSMA is superior to cabazitaxel in *PTEN*-altered mCRPC.

TP53 alterations were linked to poor PFS and OS (but not PSA50 response) independent of treatment or *TP53* allelic state (Fig. 4a–c and Supplementary Tables 8 and 9). No classes of *AR* alteration were associated with upfront resistance or differential outcomes on LuPSMA or cabazitaxel—consistent with these agents' mechanism of action not directly targeting AR signaling and earlier genomic correlative studies in taxane trials[34] (Supplementary Tables 8 and 9). Recognizing that *AR* amplifications represent a continuum, we observed that participants with ≥16 *AR* copies (top quartile) were associated with modestly shorter OS, but not PFS on LuPSMA relative to cabazitaxel when compared against all other quartiles combined (OS HR = 1.9, $P = 0.025$) (Fig. 5a and Extended Data Fig. 6). Overall, these data suggest that *AR* amplification status is not a candidate biomarker to guide treatment selection between LuPSMA and cabazitaxel.

Compromised response to DNA damage is hypothesized to predict LuPSMA outcomes[16,17]. We qualitatively explored outcomes in patients with alterations in DDR genes. Among participants with DDR alterations ($n = 46$) (Fig. 3e), the deepest (biochemical) and most durable responses to LuPSMA coincided with deleterious *ATM* (86% PSA50 response rate) and *BRCA2* (75% PSA50 response rate) alterations, including in patients with low PSMA SUVmean (Fig. 5b and Extended Data Fig. 8). Notably, two individuals with *ATM* null status experienced exceptional benefit from LuPSMA, with on-treatment PSA declining to undetectable and PFS of 30.2 and 23.1 months, respectively (although five patients with *ATM* alterations had unremarkable outcomes on LuPSMA, aligning with median PFS of all ctDNA ≥2% patients). Conversely, several patients with *CDK12* mutations benefited from cabazitaxel (only one of eight patients had primary biochemical progression), while all three patients with *CDK12*-mutated mCRPC progressed on LuPSMA before the median PFS (3.5 months; ctDNA ≥2% subset) (Fig. 5b). Outcomes appeared poor in the five individuals with DNA mismatch repair defects. Our anecdotal observations support further investigation of select DNA repair genes (particularly *ATM*) as biomarkers of LuPSMA sensitivity or resistance.

Established mCRPC driver genes rarely mediate acquired LuPSMA resistance

To explore acquired resistance, we compared baseline and progression ctDNA in participants with ctDNA ≥2% at both timepoints (85 of 106 sample pairs) (Fig. 6a and Extended Data Fig. 1). Mutational presence was highly concordant: 95% (382 of 402) of evaluable baseline mutations were redetected at progression after controlling for temporal fluctuations in ctDNA% and sequencing depth stochasticity that may precipitate false discordance (Fig. 6b and Methods). The copy number status of *TP53*, *PTEN* and *RB1* appeared stable over treatment (Extended Data Fig. 9). Genome-wide aneuploidy landscapes were highly correlated (Pearson $r = 0.91$, $P < 0.001$ in sample pairs with ≥20% ctDNA) (Fig. 6c). These data suggest that neither LuPSMA nor cabazitaxel substantially reshapes the established mCRPC genomic landscape, and are consistent with the premise that most driver defects—even those in the post third-line treatment setting—originate before metastatic dissemination[12,35,36].

We next searched for quantitative changes in per-patient mutational variant allele frequencies (VAF; adjusted for ctDNA% and copy number) indicative of treatment-induced clonal selection (Methods)[23,37]. Protein-altering mutations detected de novo at progression on LuPSMA were rare but in some cases affected *TP53* ($n = 2$), *RB1* ($n = 1$), *PTEN* ($n = 1$) and *AR* ($n = 1$) (Fig. 6b). No treatment-emergent alterations were detected in the *FOLH1*-coding region (encodes PSMA). Temporally discordant mutations were predominantly subclonal in contrast to shared mutations (median cancer cell fraction (CCF) 0.19 versus 0.81, $P < 0.001$), largely inconsistent with a complete clonal sweep (Fig. 6b). Nevertheless, most (66%) participants with ctDNA% ≥5 in both samples displayed some evidence of (sub)clonal flux on a backdrop of shared and temporally static truncal driver alterations—mainly manifesting as shifts in adjusted VAF (rather than mutation emergence or disappearance), *AR* copy number or perturbations in genome-wide aneuploidy, suggesting that LuPSMA and cabazitaxel continue to sculpt the metastatic population ecosystem.

Importantly, after incorporating all evidence, no driver gene alterations were enriched during either LuPSMA or cabazitaxel treatment (Fig. 6a–e). Although 28% of patients had significant changes in ctDNA%-adjusted *AR* copy number, inconsistent directionality suggests broader (sub)clonal shifts rather than direct selection for augmented *AR* genotypes, contrasting established evolution patterns during sequential ARPI[12,23]. There was no significant difference in *AR* gene copy number (median copies at baseline versus progression: (4.6 versus 8.1, $P = 0.6$ (LuPSMA); 3.5 versus 3.8, $P = 0.9$ (cabazitaxel)) or enhancer (6.6 versus 9.0, $P = 0.5$; 6.3 versus 4.4, $P = 1.0$), nor any enrichment for *AR* LBD mutations across timepoints (Fig. 6b,d,e). These results demonstrate that although population shifts occasionally favor clinically relevant genes (for example, *RB1*, *TP53*), treatment-induced selection for resistant clones is not singularly mediated through any common mCRPC driver genotype.

Finally, we dichotomized individuals based on evidence supporting a temporal population shift, incorporating quantitative changes in mutation clonality, *AR* copy number and genome-wide aneuploidy (Fig. 6a and Methods). Patients with a population shift had deeper PSA responses (median −50.3% versus −13.7%, $P = 0.093$) and lower frequency of primary PSA rise (23.4% versus 45.8%, $P = 0.063$), likely because of the depletion of treatment-sensitive populations and subsequent repopulation with genotypically distinct resistant clones (Fig. 6f). A weaker biochemical response in individuals without clonal shifts is compatible with a population ecosystem primed for primary resistance.

Fig. 3 | Genomic landscape of docetaxel and ARPI-treated mCRPC. a, Overview of targeted panel assay design used to sequence samples, with an exemplar of data generated from each patient sample (right). **b**, Baseline alteration frequency in key prostate cancer genes in patients with ctDNA ≥2%, showing the presence of any alteration (top) and total allelic inactivation (null) status (bottom). For *TP53* and *PTEN*, a breakdown of combinatorial mechanisms resulting in null status is provided. **c**, Mutational frequency of recurrent somatic and germline alterations compared with published cohorts[24,25,28]. Cross-cohort comparisons of *AR* gain were restricted to samples with ≥5% ctDNA given the challenges of reliably detecting *AR* gain in low ctDNA% (no post-hoc subsetting was performed on the tissue cohort). **d**, Distribution of absolute *AR* copy number and other established mechanisms of *AR* activation (*AR* genomic structural rearrangements and LBD point mutations) in 151 baseline samples with ≥2% ctDNA. Dotted gray lines at four *AR* copies represent the threshold used to define an *AR* gain. **e**, Breakdown of 46 patients with a germline and/or somatic alteration in ≥1 DNA damage repair (DDR)-related gene(s), showing co-occurrence patterns relative to other DDR genes and select non-DDR drivers (*TP53* and *PTEN*). **f**, Distribution of PSMA SUVmean (top) and FDG MTV (bottom) stratified by *PTEN* (left) and *TP53* (right) alteration status in patients with baseline ctDNA ≥2% ($n = 150$). Dashed lines represent previously established clinically relevant thresholds for high PSMA expression (SUVmean ≥10) and high FDG MTV (≥200 ml)[5]. Boxplots are accompanied by linear regression models incorporating genomic alteration status and/or ctDNA%, with the respective molecular imaging parameter constituting the independent variable. The multivariable *P* value represents a model that includes both dependent variables: alteration status and ctDNA%. **g**,**h**, Distribution of PSMA SUVmean stratified by *AR* alteration category (**g**) and alteration status in commonly affected DDR genes plus *SPOP* (MATH-domain only) and *FOXA1* (**h**). Dashed lines represent the threshold for high PSMA expression (SUVmean ≥10). del., deletion; KDE, kernel density plot; Q value, ; SV, structural variant; TTV, total tumor volume; w/o, without.

https://doi.org/10.1038/s41591-025-03704-9

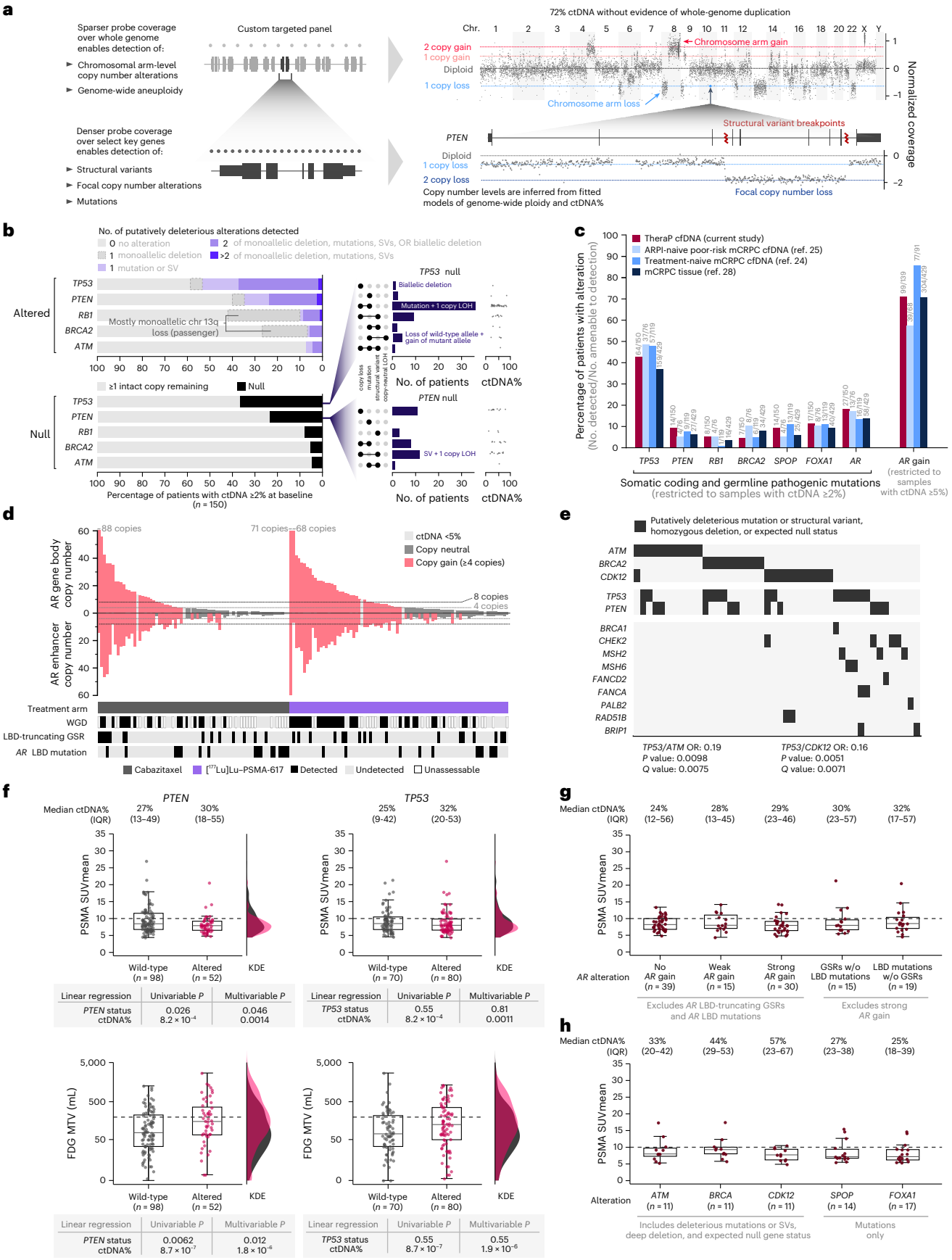

https://doi.org/10.1038/s41591-025-03704-9

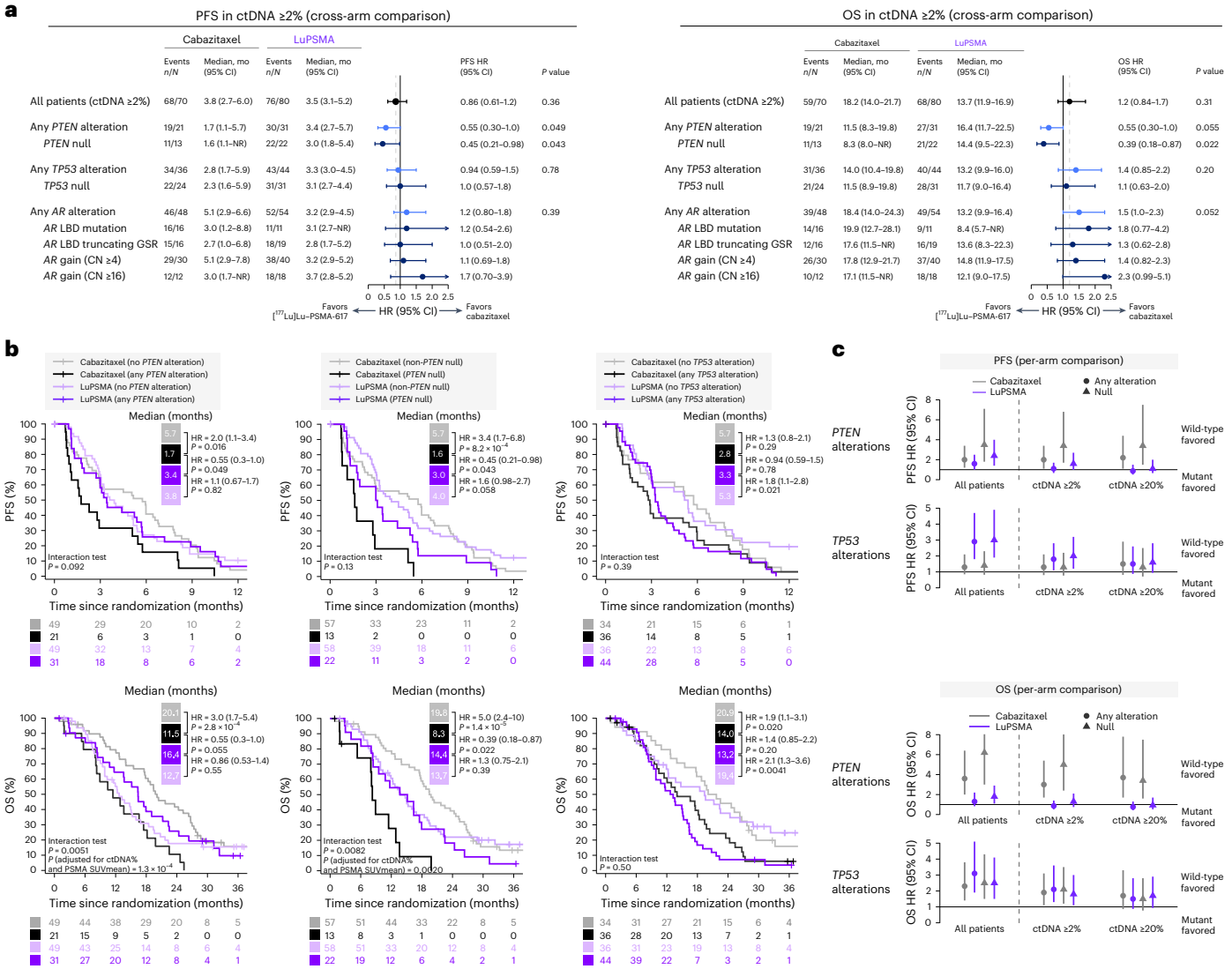

Fig. 4 | Clinical outcomes by *PTEN*, *TP53* and *AR* alteration status. a, Forest plots show post-hoc sensitivity analyses for PFS (left) and OS (right) according to baseline *PTEN*, *TP53* and *AR* alteration status in samples with ctDNA ≥2%. The 'All patients' category includes those in the biomarker population with baseline ctDNA ≥2% ($n = 150$). *AR* copy number thresholds of 4 and 16 were chosen because they represented the median and top quartile absolute *AR* copy number, respectively. HRs for each subgroup comparison represent univariable Cox proportional hazards models. Formal statistical testing was not performed for all subgroup comparisons if the overarching category (any alteration in *PTEN*, *TP53* and *AR*) was not statistically significant at an unadjusted *P* value <0.05. The exception to this was *PTEN* alterations for the OS outcome, which was formally tested because PFS was statistically significant. **b**, Kaplan–Meier estimates of PFS and OS stratified by any *PTEN* alteration (left), *PTEN* null (middle) and any *TP53* alteration (right) status. Interaction test represents the treatment interaction with the genomic alteration of interest. Adjusted multivariable interaction *P* values were generated only if univariable interaction testing showed a *P* value of <0.05. **c**, Per-arm forest plots for PFS and OS for *PTEN* and *TP53* alterations. Each plot compares alteration detected versus alteration not detected (that is, mutant versus wild-type) in each treatment arm, stratified by different ctDNA% thresholds (all patients, patients with ctDNA ≥2% ($n = 150$) and patients with ctDNA ≥20% ($n = 101$) and allelic status (null versus any alteration)). No formal statistical testing is performed. All forest plots (**a**, **c**) show HR and 95% CI. CN, copy number; mo, months.

Discussion

Our clinicogenomic analysis leveraging 290 blood samples from the prospective randomized TheraP study nominates new candidate predictive biomarkers to inform LuPSMA versus cabazitaxel treatment selection. These findings are reinforced by our incorporation of a more extensive spectrum of somatic alterations than previously studied, while controlling for the confounding effect of ctDNA% on both alteration detection sensitivity and prognosis[38]. Crucially, the real-world significance of our findings is underscored by the cabazitaxel control arm—the established alternative treatment option in this setting[39]—positioning our study as a benchmark for objective evaluation of biomarker performance in future studies. Our work endorses ctDNA genotyping as a complement to current PSMA-PET and FDG-PET selection for LuPSMA, and provides a framework for investigating circulating biomarkers for PSMA-targeting radionuclide therapeutics in clinical development (for example, actinium-225 or terbium-161)[40,41].

Pretreatment ctDNA% strongly stratified differential biochemical and PFS outcomes, with ctDNA% showing predictive potential to inform treatment selection in mCRPC. These findings also validate and extend previous noncomparative observational studies in LuPSMA-treated cohorts indicating that ctDNA% is prognostic[13,14], reaffirming its broader prognostic utility across mCRPC treatment contexts[20–22]. Patients with undetected pretreatment ctDNA unexpectedly experienced an 88% lower risk of progression with LuPSMA

https://doi.org/10.1038/s41591-025-03704-9

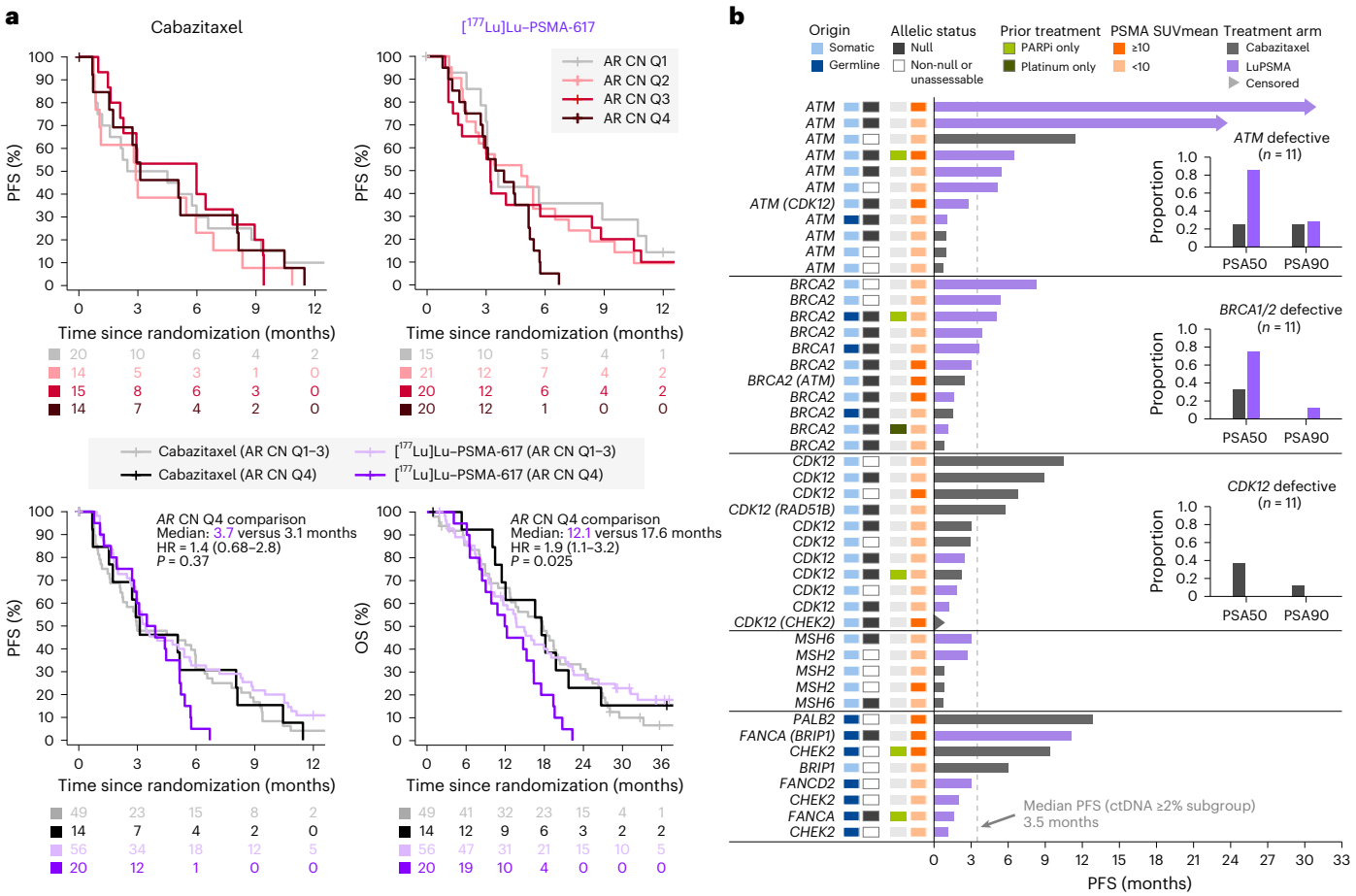

Fig. 5 | Clinical outcomes by *AR* copy number and DDR defects. a, Kaplan–Meier estimates of PFS and OS stratified by *AR* absolute copy number quartiles (top: Q1–4; bottom Q1–3 versus Q4) in patients with ctDNA ≥5%. **b**, Swimmers plot of PFS for 46 patients with evidence of a germline and/or somatic alteration in ≥1 DDR gene. Patients are grouped by DNA repair gene category: *ATM*-defective, *BRCA*1/2-defective, *CDK12*-defective, MMR-defective and Other. In each DNA repair gene-defective category, patients are ordered by PFS (longest to shortest), without accounting for censoring. Patients with >1 DDR gene alteration were grouped by their primary gene alteration, with the secondary gene alteration in parentheses (Supplementary Table 5); no patients had >2 DDR gene alterations. One patient in the *ATM*-altered category receiving cabazitaxel experienced a progressive event before recording a single on-treatment PSA value, and was therefore classified as not experiencing a PSA response in the summary bar plots. The vertical dashed line represents the median PFS of the entire biomarker-eligible ITT population with ctDNA≥2% (regardless of biomarker status), and is intended to serve as a qualitative visual benchmark. CN, absolute copy number.

compared with cabazitaxel, identifying a group of exceptional responders that cannot be predicted by high PSMA tumor uptake alone. Intriguingly, when this favorable-risk undetected ctDNA subgroup is excluded, the magnitude of PFS benefit with LuPSMA over cabazitaxel is less pronounced (PFS HR = 0.64 and 0.88 for the all-comers biomarker population and ctDNA ≥2%, respectively). Although the primary determinants of this relationship cannot be definitively established here, they may be attributable to biological characteristics captured by low ctDNA% disease, including low tumor burden, reduced proliferative capacity and higher PSMA avidity.

Despite these salient findings, undetected ctDNA encompassed a small subset of participants in TheraP (16% of biomarker population), potentially limiting broad utility in heavily pretreated disease. Furthermore, disparate outcomes favoring LuPSMA in those with undetected ctDNA did not translate to OS benefit. In contrast to the TheraP population, ctDNA is undetected in 20–43% of ARPI and/or taxane-naive mCRPC patients[24,25,42]. Recent trials demonstrating clinically meaningful LuPSMA efficacy in earlier disease[19,43] may clarify the role of ctDNA quantification in influencing treatment prioritization. Importantly, the potential for ctDNA% to guide rational treatment selection is not without precedent, as previously observed in the context of sequential ARPI[23]. Patients with low ctDNA% appear most likely to benefit from sequential ARPI—a strategy that rarely provides durable disease control in unselected mCRPC[44]—but its predictive utility (compared with docetaxel) will be clarified in a prospective ctDNA%-guided trial (NCT04015622). Notwithstanding the need for validation, our data strongly suggest that low ctDNA% should prioritize ARPI- and docetaxel-exposed mCRPC for treatment with LuPSMA over cabazitaxel, and should encourage future PSMA radioligand therapy trials to use ctDNA% as a stratification factor or as an enrichment strategy for selecting likely responders.

Assessing LuPSMA eligibility in mCRPC currently relies on detecting PSMA-positive disease via PET. Imaging-based selection offers clear strengths, including precise spatial delineation of tumor burden across anatomical regions, characterization of tumor heterogeneity, as well as provision of crucial metrics of target abundance. The culmination of these molecular imaging elements has expanded our understanding of how tissue tropism impacts LuPSMA efficacy[6,45], and accelerated development of risk stratification models in patients receiving LuPSMA[46]. Nevertheless, anticipated expansion of indications for PSMA-targeted radioligand therapy may strain efforts to broaden global access to both PET imaging and theranostic treatment alike[47]. Pending validation in independent cohorts, our ctDNA% data support the hypothesis that ctDNA testing may be a complementary triage tool

alongside PSMA-PET imaging when evaluating LuPSMA candidacy. Existing validated commercial assays capable of measuring ctDNA%[48] are now widely available (via mail-in testing), with results consistently delivered within 2–4 weeks[49,50]. Furthermore, ctDNA testing can offer additional genomic alteration status with broader relevance for treatments beyond PSMA radioligand therapy[38]. Future studies should explore approaches to implementing ctDNA% estimation into clinical workflow, balancing issues around resourcing, access and efficiency.

The relationship between genomic variables and molecular imaging indices in patients with prostate cancer has not previously been systematically investigated. ctDNA% correlated with volumetric parameters (for example, FDG MTV), as previously reported in lung cancer[51]. Intriguingly, ctDNA% was inversely correlated with PSMA SUVmean, possibly due to greater disease heterogeneity resulting in lower mean avidity. Preclinical work demonstrates that PSMA catabolism activates downstream PI3K signaling[52]. In our cohort, *PTEN* defects correlated with modestly lower PSMA SUVmean independent of ctDNA%—potentially implying that activation of downstream effectors of the PSMA-PI3K signaling cascade may trigger reciprocal negative feedback on PSMA expression—but contrasts earlier data indicating that PTEN and PSMA tissue IHC expression are not correlated[52]. Overall, our findings suggest that mCRPC driver defects (in *AR*, *TP53*, and DNA repair genes) are unlikely to serve as a strong proxy for PSMA-PET parameters, notwithstanding the minor relationship between *PTEN* and PSMA SUVmean warranting deeper investigation.

In our imaging-selected docetaxel-exposed patients treated with cabazitaxel, *PTEN* alterations were associated with significantly worse time to treatment failure and survival compared with *PTEN* wild-type—independent of ctDNA% and PSMA SUVmean—driving the apparent differential benefit of LuPSMA over cabazitaxel for *PTEN*-altered patients. This juxtaposes previous noncomparative series linking PI3K alterations to poor outcomes on LuPSMA[13–15]. In contrast to our work, these studies were unable to resolve the compounding prognostic effects of ctDNA% and genomic alteration status, reinforcing that detection of genomic alterations in cfDNA incorporates the independent prognostic influence of ctDNA%[38]. Poor PFS and OS on cabazitaxel in patients with *PTEN* deficiency is potentially compatible with its role as a negative prognostic factor in mCRPC[53], although it remains mechanistically unclear why *PTEN* alterations did not also stratify LuPSMA-treated patients. Intriguingly, *ATM* alterations were anecdotally linked to highly durable LuPSMA benefit in select patients, corroborating evidence implicating *ATM* deficiency in radiosensitivity[54]. Given the emerging consensus that PARPi are ineffective in *ATM*-deficient mCRPC[55], our result positions LuPSMA as a potential alternative treatment. Importantly, *AR* alterations were not associated with differential outcomes. Together with the lack of correlation with synchronous PSMA SUVmean and absence of selection for augmented *AR* genotypes during LuPSMA treatment, these data challenge earlier suggestions that PSMA is directly regulated by the AR and/or suggest this relationship is less prominent in ARPI-resistant mCRPC[56–58]. The neutral prognosis of *AR*-altered mCRPC on cabazitaxel and LuPSMA contrasts with that observed in the first- and second-line ARPI setting, where pretreatment *AR* genomic structural rearrangements and high-level amplifications portend upfront resistance[24,34,59]. Given recent positive results for LuPSMA trials in earlier-line mCRPC (for example, SPLASH, PSMAfore)[19,60], the apparent indifference of LuPSMA to *AR* genotype may inform eventual LuPSMA monotherapy use in settings in which ARPI is a competing alternative. Collectively, our correlative results offer renewed therapeutic decision-making strategies for mCRPC genomic subtypes (for example, *PTEN*, *ATM*, *CDK12*) that have eluded previous precision oncology efforts[55,61,62], but will require validation in other large cohorts and treatment contexts. Recognizing that distinct classes of genomic alteration can differentially impact protein function, and that functional gene dosage can influence clinical outcomes (for example, *BRCA2* homozygous versus heterozygous loss in the context of PARPi[63]), we urge future translational efforts to investigate compound allelic status utilizing the methodological blueprint herein.

No recurrent acquired resistance mechanism(s) to LuPSMA emerged in our analysis, compatible with the general expectation that resistance to anticancer agents is often heterogeneous and polyclonal. Inactivating surface receptor gene defects can precipitate treatment failure in other cancers (for example, *TROP2* vis-à-vis sacituzumab govitecan in breast cancer[64]), but no acquired *FOLH1* mutations were detected at progression on LuPSMA—compatible with recrudescence of PSMA-positive disease as a predominant progression pattern on LuPSMA[65]. There were no consistent directional changes in *AR* genotype suggestive of selection (positive or negative) during either treatment, indicating that further *AR* signaling perturbation is unlikely to be a dominant driver of acquired resistance. Frequent and occasionally pronounced temporal fluctuations in *AR* genotype plausibly reflect genetic drift driven by selection of other (possibly undetected) (epi) genotypes, compatible with previous literature indicating that the majority of mCRPC intrapatient clonal diversity is concentrated in the *AR* locus[12,23,35]. The modestly increased *AR* copy number during both therapies was not statistically significant, but would be compatible with ongoing selective pressure from the concomitant androgen deprivation therapy received by all patients.

Three patients harbored evidence for positive selection of *TP53* and/or *RB1* defects during LuPSMA, raising the possibility that these genes facilitate resistance in a minority of cancer clones and/or patients. Whether *TP53* and *RB1* defects functionally drive acquired LuPSMA resistance or merely reflect clonal flux mediated via selection

Fig. 6 | Resistance alterations. a, Summary of per-patient evidence for three categories of population shift (mutational, *AR* copy number and genome-wide large-scale aneuploidy) in 106 patients with paired baseline and progression cfDNA. Sample pairs are grouped by ctDNA% sufficiency for different analyses investigating temporal somatic changes. **b**, Mirrored bar plot of coding mutation VAF in patients with ≥2% ctDNA in both timepoints where a coding mutation was detected in targeted genes at either timepoint ($n = 83$ patients). ctDNA% is adjusted for ctDNA% and absolute copy number (CCF) at baseline (top) versus progression (bottom). Each bar (mutation) is colored by gene and grouped by detection at timepoints and significant CCF change. Boxplots summarize CCFs of mutations detected at both timepoints (two data points per mutation, one for each timepoint) versus those detected only at one timepoint (one data point per mutation). The *P* value reflects a two-sided Mann–Whitney *U*-test. **c**, Top, summary plots of genome-wide heterozygous SNP backbone coverage LR and HSAF profiles in baseline and progression, aggregated across all patients with evaluable copy number models and ≥20% ctDNA at both timepoints ($n = 44$). Bottom, per-patient genome-wide traces of significant changes in absolute copy number (red and blue) and/or heterozygous SNP allele fractions (gray) between timepoints. Only patients with five or more significant genomic changes are visualized (Methods). **d**, Absolute copy number and 95% CI (Methods) of the *AR* gene at baseline and progression in patients with ≥5% ctDNA in both timepoints ($n = 71$), stratified by treatment arm. **e**, Aggregated mean absolute *AR* copy number of patients with ≥5% ctDNA in both timepoints, stratified by treatment arm, across the *AR* enhancer, *AR* gene body and flanking regions. Each dot represents a targeted sequencing probe. 95% CIs are shown in gray for baseline and red for progression. **f**, Upper left, schematic of relationship between PSA response and clonal shift. Best PSA response waterfall plot ($n = 71$ patients) is stratified by the presence of a population shift (defined as a shift in mutational profile, *AR* copy number and/or large chromosomal copy number changes) (Methods). Lower, three case studies are highlighted with their evidence (or lack thereof) of population shift (mutations in mirrored bar plots, *AR* CN and 95% CI in whiskers below, and genome-wide aneuploidy on the right). Coding and noncoding mutations are annotated in dark gray and light gray text respectively. Evidence of change between timepoints is highlighted in pink and red; chr, chromosome; mut., mutation; MWU, Mann–Whitney *U*-test.

https://doi.org/10.1038/s41591-025-03704-9

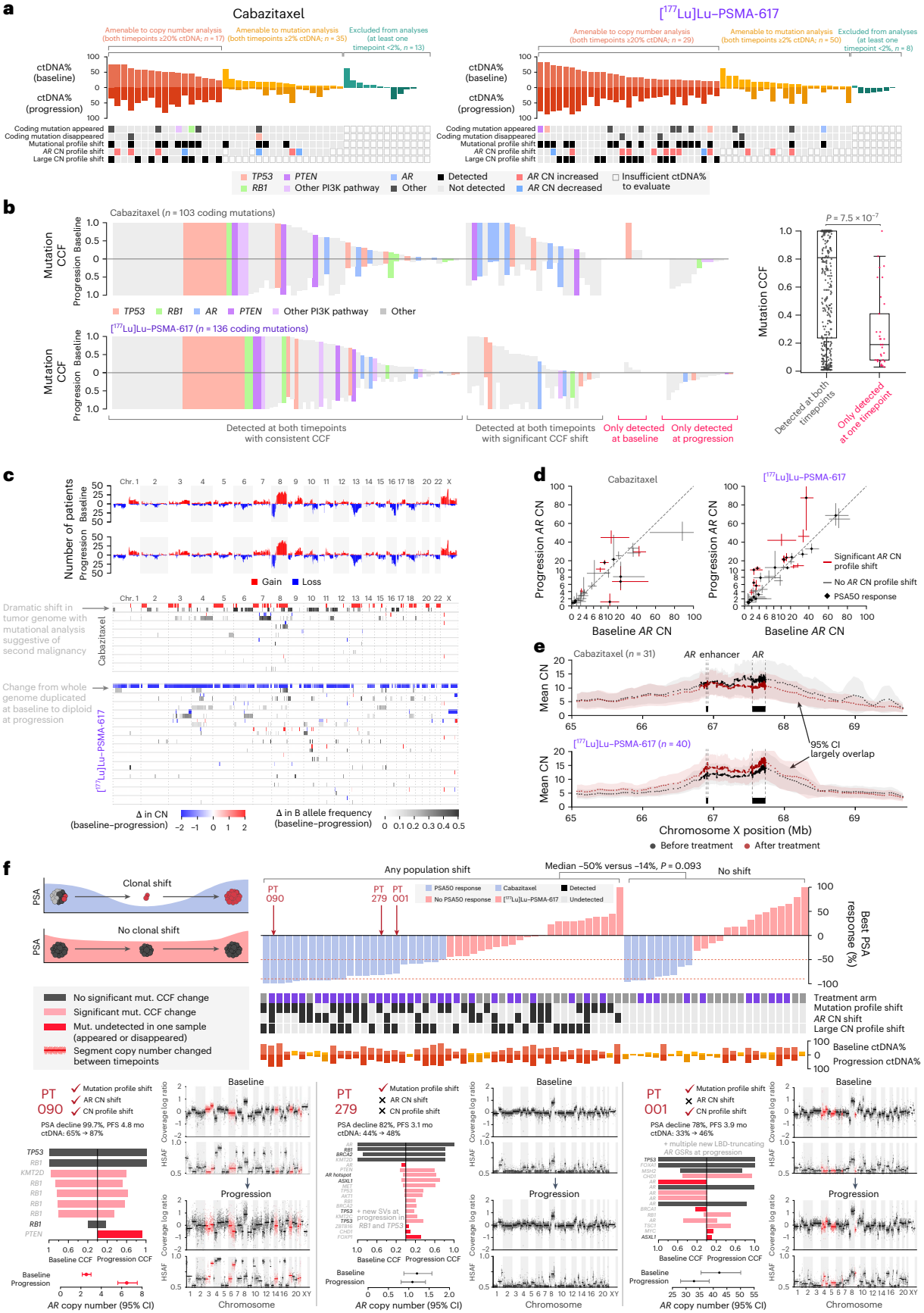

of other biological features is unclear from our data. Nevertheless, *TP53* and *RB1* are established drivers of lineage plasticity during ARPI[66], and intriguingly an epigenomic study described a case of transdifferentiation to neuroendocrine mCRPC during progression on LuPSMA[67]. Neuroendocrine prostate cancer is linked to lower PSMA avidity and higher likelihood of 2-[^{18}F]FDG-discordant disease[45,58,68], suggesting *RB1*-mediated LuPSMA resistance may be more common in patients screened using PSMA-PET alone. Collectively, these data merit further investigation of lineage dysregulation as a possible LuPSMA resistance mechanism. Quantifying spatial patterns of PSMA (with or without FDG) uptake at LuPSMA progression—plus synchronous interrogation of (epi)genomic tumor features using broader sequencing approaches (for example, deep whole-genome sequencing)—will help discover mechanisms of emergent LuPSMA resistance and is feasible in contemporaneous clinical trial datasets including ENZA-p and PRINCE[43,69].

Our study has several limitations. First, molecular imaging eligibility for TheraP enriched for high PSMA tumor uptake without 2-[^{18}F]FDG-discordant disease, differing from the registrational VISION trial for LuPSMA[3]. The biological implications of this stringent imaging preselection may limit the generalizability of our findings to settings in which FDG-PET is not used to evaluate PSMA radioligand therapy candidacy. Encouragingly, the impact of dual-tracer selection on synchronous ctDNA%-imaging and genomic-imaging biological correlatives is being addressed in the ENZA-p trial, in which all participants underwent dual PSMA-PET and FDG-PET screening, with only the former utilized for study eligibility assessment[43]. Second, observations of differential outcomes by ctDNA% and genomic features may be specific to the comparison of LuPSMA monotherapy and cabazitaxel and should not be indiscriminately extrapolated to other treatment regimens, including other taxane cytotoxics and combination therapies involving LuPSMA. These hypotheses will be explored in the Canadian Cancer Trials Group PR.21 study of LuPSMA versus docetaxel in ARPI-treated mCRPC[18], as well as in other ongoing studies evaluating LuPSMA combinations[43,69]. Third, TheraP evaluated LuPSMA in late-line mCRPC in which ctDNA is abundant. Studies in earlier disease settings[70,71] should clarify: (1) whether ctDNA% retains predictive significance in a clinical setting marked by a different (lower) ctDNA%-risk distribution; (2) whether additional substratification of the ctDNA<2% subgroup (utilizing assays with greater analytical sensitivity) may offer further outcomes discrimination; and (3) whether genomic alterations in ctDNA remain practical for outcomes prediction and detailed biological research, given that lower ctDNA% constrains resolution of certain biologically relevant alteration classes[38]. Fourth, this work is underpowered to investigate outcomes for low prevalence genomic alterations, most evident in the analysis of DDR genes. Finally, our analysis focuses exclusively on genomic biomarkers (aligning with the current capacities of widely available ctDNA companion diagnostics), but cannot address epigenomic factors, which have been recently implicated in PSMA regulation[45,72]. Multimodal strategies incorporating 5-(hydroxy)methylcytosine sequencing, cfDNA fragmentomic profiling and cell-free chromatin immunoprecipitation may refine and expand predictors of LuPSMA benefit, while more accurately identifying cancers where lineage plasticity contributes to acquired LuPSMA resistance.

We provide a comprehensive evaluation of ctDNA genomic correlatives from the first prospective randomized trial comparing LuPSMA to the active and clinically relevant control of cabazitaxel. Our data, although hypothesis-generating, offer a roadmap for biomarker development efforts for PSMA-targeting radionuclide therapeutics.

Online content

Any methods, additional references, Nature Portfolio reporting summaries, source data, extended data, supplementary information, acknowledgements, peer review information; details of author contributions and competing interests; and statements of data and code availability are available at https://doi.org/10.1038/s41591-025-03704-9.

References

1. Hofman, M. S. et al. [^{177}Lu]Lu-PSMA-617 versus cabazitaxel in patients with metastatic castration-resistant prostate cancer (TheraP): a randomised, open-label, phase 2 trial. *Lancet* **397**, 797–804 (2021).
2. Hofman, M. S. et al. Overall survival with [^{177}Lu]Lu-PSMA-617 versus cabazitaxel in metastatic castration-resistant prostate cancer (TheraP): secondary outcomes of a randomised, open-label, phase 2 trial. *Lancet Oncol.* **25**, 99–107 (2023).
3. Sartor, O. et al. Lutetium-177–PSMA-617 for metastatic castration-resistant prostate cancer. *N. Engl. J. Med.* **385**, 1091–1103 (2021).
4. Gafita, A. et al. Predictors and real-world use of prostate-specific radioligand therapy: PSMA and beyond. *Am. Soc. Clin. Oncol. Educ. Book* **42**, 1–17 (2022).
5. Buteau, J. P. et al. PSMA and FDG-PET as predictive and prognostic biomarkers in patients given [^{177}Lu]Lu-PSMA-617 versus cabazitaxel for metastatic castration-resistant prostate cancer (TheraP): a biomarker analysis from a randomised, open-label, phase 2 trial. *Lancet Oncol.* **23**, 1389–1397 (2022).
6. Kuo, P. H. et al. Quantitative ^{68}Ga-PSMA-11 PET and clinical outcomes in metastatic castration-resistant prostate cancer following ^{177}Lu-PSMA-617 (VISION trial). *Radiology* **312**, e233460 (2024).
7. Thang, S. P. et al. Poor outcomes for patients with metastatic castration-resistant prostate cancer with low prostate-specific membrane antigen (PSMA) expression deemed ineligible for ^{177}Lu-labelled PSMA radioligand therapy. *Eur. Urol. Oncol.* **2**, 670–676 (2019).
8. de Bono, J. et al. Olaparib for metastatic castration-resistant prostate cancer. *N. Engl. J. Med.* **382**, 2091–2102 (2020).
9. Abida, W. et al. Analysis of the prevalence of microsatellite instability in prostate cancer and response to immune checkpoint blockade. *JAMA Oncol.* **5**, 471–478 (2019).
10. Hussain, M. et al. Tumor genomic testing for >4000 men with metastatic castration-resistant prostate cancer in the phase III trial PROfound (Olaparib). *Clin. Cancer Res.* **28**, 1518–1530 (2022).
11. Kwan, E. M., Wyatt, A. W. & Chi, K. N. Towards clinical implementation of circulating tumor DNA in metastatic prostate cancer: opportunities for integration and pitfalls to interpretation. *Front. Oncol.* **12**, 1054497 (2022).
12. Herberts, C. et al. Deep whole-genome ctDNA chronology of treatment-resistant prostate cancer. *Nature* **608**, 199–208 (2022).
13. Fettke, H. et al. Abstract 5614: Genomic aberrations in circulating tumor DNA (ctDNA) and clinical outcomes from [^{177}Lu] Lu-PSMA-617 in metastatic castration-resistant prostate cancer (mCRPC). *Cancer Res.* **83**, 5614 (2023).
14. Vanwelkenhuyzen, J. et al. AR and PI3K genomic profiling of cell-free DNA can identify poor responders to lutetium-177-PSMA among patients with metastatic castration-resistant prostate cancer. *Eur. Urol. Open Sci.* **53**, 63–66 (2023).
15. Crumbaker, M. et al. Circulating tumour DNA biomarkers associated with outcomes in metastatic prostate cancer treated with lutetium-177-PSMA-617. *Eur. Urol. Open Sci.* **57**, 30–36 (2023).
16. Sartor, O. et al. Prediction of resistance to ^{177}Lu-PSMA therapy by assessment of baseline circulating tumor DNA biomarkers. *J. Nucl. Med.* **64**, 1721–1725 (2023).
17. Raychaudhuri, R. et al. Genomic correlates of prostate-specific membrane antigen expression and response to ^{177}Lu-PSMA-617: a retrospective multicenter cohort study. *JCO Precis. Oncol.* **8**, e2300634 (2024).

18. Chi, K. N. et al. CCTG PR21: a randomized phase II study of [^{177}Lu]Lu-PSMA-617 verus docetaxel in patients with metastatic castration-resistant prostate cancer and PSMA-positive disease (NCT04663997). *J. Clin. Oncol.* **40**, TPS5110 (2022).
19. Morris, M. J. et al. Lu-PSMA-617 versus a change of androgen receptor pathway inhibitor therapy for taxane-naive patients with progressive metastatic castration-resistant prostate cancer (PSMAfore): a phase 3, randomised, controlled trial. *Lancet* **404**, 1227–1239 (2024).
20. Fonseca, N. M. et al. Prediction of plasma ctDNA fraction and prognostic implications of liquid biopsy in advanced prostate cancer. *Nat. Commun.* **15**, 1828 (2024).
21. Tolmeijer, S. H. et al. Early on-treatment changes in circulating tumor DNA fraction and response to enzalutamide or abiraterone in metastatic castration-resistant prostate cancer. *Clin. Cancer Res.* **29**, 2835–2844 (2023).
22. Choudhury, A. D. et al. Tumor fraction in cell-free DNA as a biomarker in prostate cancer. *JCI Insight* **3**, e122109 (2018).
23. Annala, M. et al. Evolution of castration-resistant prostate cancer in ctDNA during sequential androgen receptor pathway inhibition. *Clin. Cancer Res.* **27**, 4610–4623 (2021).
24. Annala, M. et al. Circulating tumor DNA genomics correlate with resistance to abiraterone and enzalutamide in prostate cancer. *Cancer Discov.* **8**, 444–457 (2018).
25. Annala, M. et al. Cabazitaxel versus abiraterone or enzalutamide in poor prognosis metastatic castration-resistant prostate cancer: a multicentre, randomised, open-label, phase 2 trial. *Ann. Oncol.* **32**, 896–905 (2021).
26. Ferdinandus, J. et al. Prognostic biomarkers in men with metastatic castration-resistant prostate cancer receiving [^{177}Lu]-PSMA-617. *Eur. J. Nucl. Med. Mol. Imaging* **47**, 2322–2327 (2020).
27. Quigley, D. A. et al. Genomic hallmarks and structural variation in metastatic prostate cancer. *Cell* **175**, 889 (2018).
28. Abida, W. et al. Genomic correlates of clinical outcome in advanced prostate cancer. *Proc. Natl Acad. Sci. USA* **116**, 11428–11436 (2019).
29. Chakraborty, G. et al. The impact of PIK3R1 mutations and insulin-PI3K-glycolytic pathway regulation in prostate cancer. *Clin. Cancer Res.* **28**, 3603–3617 (2022).
30. De Laere, B. et al. *TP53* outperforms other androgen receptor biomarkers to predict abiraterone or enzalutamide outcome in metastatic castration-resistant prostate cancer. *Clin. Cancer Res.* **25**, 1766–1773 (2019).
31. De Laere, B. et al. Androgen receptor burden and poor response to abiraterone or enzalutamide in TP53 wild-type metastatic castration-resistant prostate cancer. *JAMA Oncol.* **5**, 1060–1062 (2019).
32. Fettke, H. et al. Combined cell-free DNA and RNA profiling of the androgen receptor: clinical utility of a novel multianalyte liquid biopsy assay for metastatic prostate cancer. *Eur. Urol.* **78**, 173–180 (2020).
33. Kwan, E. M. et al. Plasma cell-free DNA profiling of PTEN-PI3K-AKT pathway aberrations in metastatic castration-resistant prostate cancer. *JCO Precis. Oncol.* **5**, 622–637 (2021).
34. Tolmeijer, S. H. et al. A systematic review and meta-analysis on the predictive value of cell-free DNA-based androgen receptor copy number gain in patients with castration-resistant prostate cancer. *JCO Precis. Oncol.* **4**, 714–729 (2020).
35. Gundem, G. et al. The evolutionary history of lethal metastatic prostate cancer. *Nature* **520**, 353–357 (2015).
36. Warner, E. W. et al. Multiregion sampling of de novo metastatic prostate cancer reveals complex polyclonality and augments clinical genotyping. *Nat. Cancer* **5**, 114–130 (2024).
37. McGranahan, N. et al. Clonal status of actionable driver events and the timing of mutational processes in cancer evolution. *Sci. Transl. Med.* **7**, 283ra54 (2015).
38. Herberts, C. & Wyatt, A. W. Technical and biological constraints on ctDNA-based genotyping. *Trends Cancer Res.* **7**, 995–1009 (2021).
39. de Wit, R. et al. Cabazitaxel versus abiraterone or enzalutamide in metastatic prostate cancer. *N. Engl. J. Med.* **381**, 2506–2518 (2019).
40. Jang, A., Kendi, A. T., Johnson, G. B., Halfdanarson, T. R. & Sartor, O. Targeted alpha-particle therapy: a review of current trials. *Int. J. Mol. Sci.* **24**, 11626 (2023).
41. Buteau, J. P. et al. Clinical trial protocol for VIOLET: a single-center, phase I/II trial evaluation of radioligand treatment in patients with metastatic castration-resistant prostate cancer with [^{161}Tb]Tb-PSMA-I&T. *J. Nucl. Med.* **65**, 1231–1238 (2024).
42. Sumanasuriya, S. et al. Elucidating prostate cancer behaviour during treatment via low-pass whole-genome sequencing of circulating tumour DNA. *Eur. Urol.* **80**, 243–253 (2021).
43. Emmett, L. et al. [Lu]Lu-PSMA-617 plus enzalutamide in patients with metastatic castration-resistant prostate cancer (ENZA-p): an open-label, multicentre, randomised, phase 2 trial. *Lancet Oncol.* **25**, 563–571 (2024).
44. Khalaf, D. J. et al. Optimal sequencing of enzalutamide and abiraterone acetate plus prednisone in metastatic castration-resistant prostate cancer: a multicentre, randomised, open-label, phase 2, crossover trial. *Lancet Oncol.* **20**, 1730–1739 (2019).
45. Bakht, M. K. et al. Landscape of prostate-specific membrane antigen heterogeneity and regulation in AR-positive and AR-negative metastatic prostate cancer. *Nat. Cancer* **4**, 699–715 (2023).
46. Gafita, A. et al. Validation of prognostic and predictive models for therapeutic response in patients treated with [^{177}Lu]Lu-PSMA-617 versus cabazitaxel for metastatic castration-resistant prostate cancer (TheraP): a post hoc analysis from a randomised, open-label, phase 2 trial. *Eur. Urol. Oncol.* **8**, 21–28 (2024).
47. Abdel-Wahab, M. et al. Radiotherapy and theranostics: a Lancet Oncology Commission. *Lancet Oncol.* **25**, e545–e580 (2024).
48. Tukachinsky, H. et al. Genomic analysis of circulating tumor DNA in 3,334 patients with advanced prostate cancer identifies targetable BRCA alterations and AR resistance mechanisms. *Clin. Cancer Res.* **27**, 3094–3105 (2021).
49. Nakamura, Y. et al. Clinical utility of circulating tumor DNA sequencing in advanced gastrointestinal cancer: SCRUM-Japan GI-SCREEN and GOZILA studies. *Nat. Med.* **26**, 1859–1864 (2020).
50. Kwan, E. M. et al. Prospective ctDNA genotyping for treatment selection in metastatic castration-resistant prostate cancer (mCRPC): The Canadian Cancer Trials Group phase II PC-BETS umbrella study. *J. Clin. Oncol.* **41**, 218 (2023).
51. Jee, J. et al. Overall survival with circulating tumor DNA-guided therapy in advanced non-small-cell lung cancer. *Nat. Med.* **28**, 2353–2363 (2022).
52. Kaittanis, C. et al. Prostate-specific membrane antigen cleavage of vitamin B9 stimulates oncogenic signaling through metabotropic glutamate receptors. *J. Exp. Med.* **215**, 159–175 (2018).
53. Rescigno, P. et al. Docetaxel treatment in PTEN- and ERG-aberrant metastatic prostate cancers. *Eur. Urol. Oncol.* **1**, 71–77 (2018).
54. Pitter, K. L. et al. Pathogenic ATM mutations in cancer and a genetic basis for radiotherapeutic efficacy. *J. Natl Cancer Inst.* **113**, 266–273 (2021).
55. Fallah, J. et al. Efficacy of poly(ADP-ribose) polymerase inhibitors by individual genes in homologous recombination repair gene-mutated metastatic castration-resistant prostate cancer: a US Food and Drug Administration pooled analysis. *J. Clin. Oncol.* **42**, 1687–1698 (2024).
56. Hope, T. A. et al. ^{68}Ga-PSMA-11 PET imaging of response to androgen receptor inhibition: first human experience. *J. Nucl. Med.* **58**, 81–84 (2017).

57. Emmett, L. et al. Rapid modulation of PSMA expression by androgen deprivation: serial ^{68}Ga-PSMA-11 PET in men with hormone-sensitive and castrate-resistant prostate cancer commencing androgen blockade. *J. Nucl. Med.* **60**, 950–954 (2018).
58. Bakht, M. K. & Beltran, H. Biological determinants of PSMA expression, regulation and heterogeneity in prostate cancer. *Nat. Rev. Urol.* **22**, 26–45 (2024).
59. Zivanovic, A. et al. Co-evolution of *AR* gene copy number and structural complexity in endocrine therapy resistant prostate cancer. *NAR Cancer* **5**, zcad045 (2023).
60. Chi, K. N. et al. Study evaluating metastatic castrate resistant prostate cancer (mCRPC) treatment using ^{177}Lu-PNT2002 PSMA therapy after second-line hormonal treatment (SPLASH). *J. Clin. Oncol.* **39**, TPS5087 (2021).
61. Sweeney, C. et al. Ipatasertib plus abiraterone and prednisolone in metastatic castration-resistant prostate cancer (IPATential150): a multicentre, randomised, double-blind, phase 3 trial. *Lancet* **398**, 131–142 (2021).
62. Nguyen, B. et al. Pan-cancer analysis of CDK12 alterations identifies a subset of prostate cancers with distinct genomic and clinical characteristics. *Eur. Urol.* **78**, 671–679 (2020).
63. Carreira, S. et al. Biomarkers associating with PARP inhibitor benefit in prostate cancer in the TOPARP-B trial. *Cancer Discov.* **11**, 2812–2827 (2021).
64. Coates, J. T. et al. Parallel genomic alterations of antigen and payload targets mediate polyclonal acquired clinical resistance to sacituzumab govitecan in triple-negative breast cancer. *Cancer Discov.* **11**, 2436–2445 (2021).
65. Violet, J. et al. Long-term follow-up and outcomes of retreatment in an expanded 50-patient single-center phase II prospective trial of ^{177}Lu-PSMA-617 theranostics in metastatic castration-resistant prostate cancer. *J. Nucl. Med.* **61**, 857–865 (2020).
66. Ku, S. Y. et al. Rb1 and Trp53 cooperate to suppress prostate cancer lineage plasticity, metastasis, and antiandrogen resistance. *Science* **355**, 78–83 (2017).
67. Sipola, J. et al. Plasma cell-free DNA chromatin immunoprecipitation profiling depicts phenotypic and clinical heterogeneity in advanced prostate cancer. *Cancer Res.* **85**, 791–807 (2025).
68. Iravani, A. et al. Molecular imaging of neuroendocrine differentiation of prostate cancer: a case series. *Clin. Genitourin. Cancer* **19**, e200–e205 (2021).
69. Sandhu, S. et al. PRINCE: phase I trial of ^{177}Lu-PSMA-617 in combination with pembrolizumab in patients with metastatic castration-resistant prostate cancer (mCRPC). *J. Clin. Oncol.* **40**, 5017 (2022).
70. Azad, A. A. et al. Sequential [Lu]Lu-PSMA-617 and docetaxel versus docetaxel in patients with metastatic hormone-sensitive prostate cancer (UpFrontPSMA): a multicentre, open-label, randomised, phase 2 study. *Lancet Oncol.* **25**, 1267–1276 (2024).
71. Tagawa, S. T. et al. PSMAddition: a phase 3 trial to compare treatment with ^{177}Lu-PSMA-617 plus standard of care (SoC) and SoC alone in patients with metastatic hormone-sensitive prostate cancer. *J. Clin. Oncol.* **41**, TPS5116 (2023).
72. Sayar, E. et al. Reversible epigenetic alterations mediate PSMA expression heterogeneity in advanced metastatic prostate cancer. *JCI Insight* **8**, e162907 (2023).

Publisher's note Springer Nature remains neutral with regard to jurisdictional claims in published maps and institutional affiliations.

Springer Nature or its licensor (e.g. a society or other partner) holds exclusive rights to this article under a publishing agreement with the author(s) or other rightsholder(s); author self-archiving of the accepted manuscript version of this article is solely governed by the terms of such publishing agreement and applicable law.

© The Author(s), under exclusive licence to Springer Nature America, Inc. 2025

Edmond M. Kwan[1,2,3,44], Sarah W. S. Ng[1,44], Sofie H. Tolmeijer[1], Louise Emmett[4,5,6], Shahneen Sandhu[7,8], James P. Buteau[7,8], Amir Iravani[7,8,9,10], Anthony M. Joshua[5,6,11], Roslyn J. Francis[12,13], Vinod Subhash[14], Sze-Ting Lee[15,16,17,18], Andrew M. Scott[15,16,17,18], Andrew J. Martin[19,20], Martin R. Stockler[20,21], Gráinne Donnellan[1], Matti Annala[22], Cameron Herberts[1], Ian D. Davis[2,23,45] ✉, Michael S. Hofman[7,8,45] ✉, Arun A. Azad[7,8,45] ✉ & Alexander W. Wyatt[1,24,45] ✉, on behalf of the TheraP Investigators and the ANZUP Cancer Trials Group[14]*

[1]Vancouver Prostate Centre, Department of Urologic Sciences, University of British Columbia, Vancouver, British Columbia, Canada. [2]Eastern Health Clinical School, Monash University, Melbourne, Victoria, Australia. [3]Biomedicine Discovery Institute Cancer Program, Prostate Cancer Research Group, Department of Anatomy and Developmental Biology, Monash University, Melbourne, Victoria, Australia. [4]Department of Theranostics and Nuclear Medicine, St Vincent's Hospital, Sydney, New South Wales, Australia. [5]School of Clinical Medicine, Faculty of Medicine and Health, University of New South Wales, Sydney, New South Wales, Australia. [6]Garvan Institute of Medical Research, Sydney, New South Wales, Australia. [7]Prostate Cancer Theranostics and Imaging Centre of Excellence (ProsTIC), Molecular Imaging and Therapeutic Nuclear Medicine, Cancer Imaging, Peter MacCallum Cancer Centre, Melbourne, Victoria, Australia. [8]Sir Peter MacCallum Department of Oncology, The University of Melbourne, Melbourne, Victoria, Australia. [9]Division of Nuclear Medicine, Department of Radiology, University of Washington School of Medicine, Seattle, WA, USA. [10]Fred Hutchinson Cancer Center, Seattle, WA, USA. [11]Department of Medical Oncology, Kinghorn Cancer Centre, Sydney, New South Wales, Australia. [12]Department of Nuclear Medicine, Sir Charles Gairdner Hospital, Perth, Western Australia, Australia. [13]Medical School, University of Western Australia, Perth, Western Australia, Australia. [14]Australian and New Zealand Urogenital and Prostate Cancer Trials Group (ANZUP), Sydney, New South Wales, Australia. [15]Department of Medicine, The University of Melbourne, Melbourne, Victoria, Australia. [16]Department of Molecular Imaging and Therapy, Austin Health, Melbourne, Victoria, Australia. [17]School of Cancer Medicine, La Trobe University, Melbourne, Victoria, Australia. [18]Olivia Newton-John Cancer Research Institute, Melbourne, Victoria, Australia. [19]NHMRC Clinical Trials Centre, University of Sydney, Sydney, New South Wales, Australia. [20]Centre for Clinical Research, University of Queensland, Brisbane, Queensland, Australia. [21]Department of Medical Oncology, Chris O'Brien Lifehouse, Sydney, New South Wales, Australia. [22]Faculty of Medicine and Health Technology, Tampere University and Tays Cancer Centre, Tampere, Finland. [23]Cancer Services, Eastern Health, Melbourne, Victoria, Australia. [24]Michael Smith Genome Sciences Centre, BC Cancer, Vancouver, British Columbia, Canada. [44]These authors contributed equally: Edmond M. Kwan, Sarah W. S. Ng. [45]These authors jointly supervised this work: Ian D. Davis, Michael S. Hofman, Arun A. Azad, Alexander W. Wyatt. *A list of authors and their affiliations appears at the end of the paper. ✉e-mail: ian.davis@monash.edu; michael.hofman@petermac.org; arun.azad@petermac.org; alexander.wyatt@ubc.ca

The TheraP Investigators and the ANZUP Cancer Trials Group

Edmond M. Kwan[1,2,3,44], Louise Emmett[4,5,6], Shahneen Sandhu[7,8], James P. Buteau[7,8], Amir Iravani[7,8,9,10], Anthony M. Joshua[5,6,11], Roslyn J. Francis[12,13], Vinod Subhash[14], Sze-Ting Lee[15,16,17,18], Andrew M. Scott[15,16,17,18], Andrew J. Martin[19,20], Martin R. Stockler[20,21], Ian D. Davis[2,23,45], Michael S. Hofman[7,8,45], Arun A. Azad[7,8,45], Alexander W. Wyatt[1,24,45], Tim Akhurst[7], Ramin Alipour[7,8], Dale L. Bailey[25], Patricia Banks[8], Alexis Beaulieu[7], Louise Campbell[26], Wei Chua[27], Megan Crumbaker[5,6,11], Nattakorn Dhiantravan[7], Kate Ford[19], Craig Gedye[28], Jeffrey C. Goh[29], Alex D. Guminski[30], Anis Hamid[31], Mohammad B. Haskali[7,8], Rodney J. Hicks[8], Edward Hsiao[25], Terry Hung[12], Ian D. Kirkwood[32], Grace Kong[7,8], Ailsa Langford[19], Nicola Lawrence[33], Jeremy Lewin[8], Peter Lin[34], Michael McCarthy[35], Margaret M. McJannett[14], William McDonald[35], Kate Moodie[7], Declan G. Murphy[7,8], Siobhan Ng[36], Andrew Nguyen[4,5], David A. Pattison[26], David Pook[37], Izabella Pokorski[19], Shakher Ramdave[38], Nisha Rana[14], Aravind S. Ravi Kumar[7], Andrew D. Redfern[13,39], Paul Roach[25], Peter Roselt[7], Natalie K. Rutherford[40], Javad Saghebi[7,8], Geoffrey Schembri[25], Lavinia Spain[8], Shalini Subramaniam[19], Thean Hsiang Tan[41], Sue Ping Thang[7], Paul Thomas[26], Ben Tran[8], John A. Violet[7], Roslyn Wallace[8], Andrew Weickhardt[42], Scott G. Williams[8], Sonia Yip[19] & Alison Y. Zhang[43]

[25]Department of Nuclear Medicine, Royal North Shore Hospital, Sydney, New South Wales, Australia. [26]Department of Nuclear Medicine and Specialised PET Services, Royal Brisbane and Women's Hospital, Brisbane, Queensland, Australia. [27]Liverpool Cancer Therapy Centre, Liverpool Hospital, Sydney, New South Wales, Australia. [28]Department of Medical Oncology, Calvary Mater Newcastle, Waratah, New South Wales, Australia. [29]Department of Medical Oncology, Royal Brisbane and Women's Hospital, Brisbane, Queensland, Australia. [30]Royal North Shore Hospital, Sydney, New South Wales, Australia. [31]Genitourinary Oncology Service, Memorial Sloan Kettering Cancer Center, New York, NY, USA. [32]Nuclear Medicine, PET and Bone Densitometry, Royal Adelaide Hospital, Adelaide, South Australia, Australia. [33]Auckland Cancer and Blood Service, Te Whatu Ora Te Toka Tumai, Auckland, New Zealand. [34]Department of Nuclear Medicine and PET, Liverpool Hospital, Sydney, New South Wales, Australia. [35]Department of Nuclear Medicine, Fiona Stanley Hospital, Perth, Western Australia, Australia. [36]Department of Oncology, Sir Charles Gairdner Hospital, Perth, Western Australia, Australia. [37]Department of Medical Oncology, Monash Health, Melbourne, Victoria, Australia. [38]Monash Health Imaging, Monash Health, Melbourne, Victoria, Australia. [39]Department of Medical Oncology, Fiona Stanley Hospital, Perth, Western Australia, Australia. [40]Department of Nuclear Medicine, Hunter New England Health, Newcastle, New South Wales, Australia. [41]Department of Medical Oncology, Royal Adelaide Hospital, Adelaide, South Australia, Australia. [42]Olivia Newton-John Cancer and Wellness Centre, Austin Health, Melbourne, Victoria, Australia. [43]Macquarie University Hospital, Sydney, New South Wales, Australia.

Methods

Study design, participants and ethical oversight

The clinical trial study design and participant eligibility criteria have been described in detail previously[1,2,5,46]. TheraP (NCT03042312, ACTRN12615000912583) was an open-label, randomized (1:1), phase 2 trial comparing intravenous LuPSMA (every 6 weeks for a maximum of six cycles; starting at 8.5 GBq, decreasing by 0.5 GBq to 6.0 GBq for the sixth cycle) with intravenous cabazitaxel (20 mg m^{-2} every 3 weeks for a maximum of ten cycles). Eligible participants had progressive mCRPC previously treated with docetaxel and in whom cabazitaxel was considered the next appropriate standard treatment; Eastern Cooperative Oncology Group (ECOG) performance status 0 to 2; and with adequate renal, hematological and liver function. Patients were additionally selected based on the presence of PSMA-positive disease utilizing both [^{68}Ga]Ga–PSMA-11 and 2-[^{18}F]FDG-PET. Patients were required to have at least one lesion with an SUVmax ≥20, and all other measurable lesions to have an SUVmax >10. Furthermore, patients were excluded if any lesions demonstrated uptake of 2-[^{18}F]FDG without corresponding PSMA expression. Randomization was stratified for disease burden (>20 disease sites versus ≤20 disease sites as assessed by [^{68}Ga]Ga–PSMA-11), previous treatment with either enzalutamide or abiraterone and study site. The primary endpoint was PSA response (PSA50), with key secondary endpoints of PFS and OS. All participants provided signed, written, informed consent. The protocol was approved at each participating institution, and the trial was done in accordance with the principles of the Good Clinical Practice guidelines and the Declaration of Helsinki. Sex and/or gender are not relevant for any findings in this study and were therefore not incorporated into study design, clinical data collection or execution of any analyses. Prostate cancer only affects individuals born as biological males, and our cohort includes participants with aggressive prostate cancer irrespective of gender identity. All samples are deidentified at time of collection, and all researchers are blind to gender identity and gender presentation. Patients were not compensated for their participation in the TheraP trial or secondary correlative biomarker studies.

Clinical endpoints, statistical analyses and reproducibility

Given the paucity of validated predictive genomic biomarkers for either LuPSMA or cabazitaxel, the analyses herein are predominantly exploratory and hypothesis-generating. Exact sample sizes and power calculations were not formally prespecified. A core consideration informing our analysis strategy is recognition that the phase 2 TheraP trial was not formally designed to detect cross-arm differences in PFS or OS (both secondary endpoints)[1,73]. We therefore adopted a highly conservative and selective approach to our exploratory post-hoc biomarker analyses, minimizing risks associated with excessive hypothesis testing of small groups in this underpowered trial context. This includes: (1) only evaluating candidate genomic biomarkers present in ≥10% of the TheraP baseline population; (2) selective evaluation of specific alteration classes with established clinical or biological significance in mCRPC; and (3) utilizing a gated two-tiered hypothesis testing strategy that first evaluated binary alteration presence or absence in specific genes, and only stratifying by smaller biologically informed subcategories if the overall binary dichotomization was statistically significant. Statistical analyses are reported without correction for multiple testing unless otherwise stated. The rationale for patient or sample exclusion from specific sub-analyses is clearly indicated in the text and/or figure caption. We did not perform any analyses requiring randomization (beyond that originally implemented in the underlying trial).

Clinical endpoints evaluated in this study included PSA response rate, PFS and OS; extended definitions for these endpoints have been described previously[73]. PSA response rate was defined as the proportion of participants with a PSA reduction of ≥50% from baseline. PFS is defined as the interval from the date of randomization to the date of first evidence of PSA progression (as per Prostate Cancer Working Group 3 criteria), pain progression, radiographic progression, death from any cause, whichever occurs first, or the date of last known follow-up without progression. OS is defined as the interval from the date of registration to date of death from any cause or date of last known follow-up alive.

Statistical tests and data analysis were performed in R v.4.4.0 (using dplyr v.1.1.4, forcats v.1.0.0, janitor 2.2.0, lubridate v.1.9.3, purr v.1.0.2, psych v.2.4.3, stringr v.1.5.1, stats v.4.4.0, gtsummary v.1.7.2, survival v.3.5-8) and in Python 3.9.12 (using pandas v.1.4.2, numpy v.1.23.5, scipy v.1.10.1, statsmodels v.0.13.5) and Julia v.1.8.5. Visualizations were generated using the R packages ggplot2 v.3.4.3, forestplot v.3.1.3, survminer v.0.4.9, cowplot v.1.1.3 and patchwork v.1.2.0, and the Python packages matplotlib v.3.7.1 and seaborn v.0.13.0. The following bioinformatics or genomic analysis software was used: cutadapt v.4.9, seqkit v.0.8.1, Bowtie2 v.2.3.4.3, samblaster v.0.1.24, bedtools v.2.26, samtools v.1.8 (htslib v.1.8), Mutato v.0.8 and ANNOVAR (v.20191024), as well as custom in-house software. Data were presented descriptively as proportions, medians and their respective ranges. All boxplots are centered at the median unless otherwise specified and display the IQR. Whiskers extend 1.5× IQR past the quartiles; all raw data are shown where possible. Categorical variables between genomic and clinical subgroups were compared using Fisher's exact test, whereas continuous variables were compared using the Mann–Whitney *U*-test. Survival fractions for time-to-event outcomes (PFS and OS) were estimated using the Kaplan–Meier method and differences between groups were evaluated using the log rank test. Cox proportional hazards models were used to calculate hazard ratios (HR) and 95% confidence intervals (CI). All hypothesis tests were two-tailed and used a 5% significance threshold. *P* values are reported to two significant figures.

The silhouette, test tube and torso skeleton (Fig. 1a) were manipulated from the linked source and are available under a Creative Commons Attribution 2.5 Generic (https://creativecommons.org/licenses/by/2.5/) licence. We thank all the original authors for making their work available.

Blood processing and cfDNA extraction

Full details relating to sample collection and initial processing can be found in the TheraP biospecimen sampling manual (Supplementary Information). Briefly, up to 25 ml of peripheral blood was collected in EDTA collection tubes. Whole blood (up to 5 ml) was separately aliquoted, while the remaining blood (up to 20 ml) underwent two-step centrifugation (1,600*g* for 10–15 min followed by 3,000*g* for 10–15 min) to separate and clarify plasma. Plasma and whole blood were stored at −70 °C until batch sample processing.

From the whole blood sample, WBC DNA (serving as germline DNA and clonal hematopoiesis control) was isolated using the Promega Maxwell RSC Blood DNA kit (Promega; cat. no. 55114) as per the instructions outlined in the technical manual (version TM419), resulting in a final elution volume of 50 µl. Conversely, cfDNA was extracted from plasma using the QIAGEN QIAamp Circulating Nucleic Acid Kit (Qiagen) according to the manufacturer's instructions. Following extractions, WBC DNA and cfDNA were quantified using the QuantiFluor ONE dsDNA kit and Quantus Fluorometer (Promega). cfDNA samples with total cfDNA yield exceeding 50 ng ml^{-1} of plasma underwent gel electrophoresis (using 1.3% SYBR-Safe agarose gel) to rule out the presence of high molecular weight DNA resulting from probable WBC contamination. In rare instances in which high molecular weight DNA is detected (suggesting substantial admixture of WBC DNA with cfDNA), AMPure XP bead (Beckman Coulter; cat. no. A63880) clean-up was performed as per manufacturer's instructions.

Targeted capture, sequencing and bioinformatic analysis

Library preparation, targeted capture and sequencing. Sequencing libraries for WBC DNA samples were prepared with the KAPA HyperPlus Kit (Roche; cat. no. KK8512-07962401001) following instructions outlined in the technical manual (version KR1145, v.9.23): 50 ng of input DNA was used for each library. Enzymatic fragmentation of WBC DNA was performed for 15 min at 37 °C using a diluted conditioning solution resulting in a final concentration of 0.06 mM EDTA in the fragmentation reaction. Sequencing libraries for cfDNA samples were prepared with the KAPA HyperPrep Kit (Roche) as per the manufacturer's instructions: 10–50 ng input cfDNA was used for each library, depending on cfDNA extraction yield (Supplementary Table 2). After end-repair and A-tailing, both WBC DNA and cfDNA libraries underwent overnight adapter ligation at 4 °C using IDT xGen CS UMI Adapters (IDT; cat. no. 1080799), followed by polymerase chain reaction amplification with custom unique dual index primer pairs. Library quantification was performed via NanoDrop, and each library was run on a 1.3% SYBR-Safe agarose gel to confirm success.

Purified sample libraries were multiplexed to obtain single pools with a combined mass of 2.5 µg. Library pools were then hybridized to a KAPA HyperChoice probe set for a minimum of 16 h at 55 °C. This probe set has previously been described[21]. In brief, it captures exons from 76 predominantly prostate cancer-relevant genes (including *FOLH1*, which encodes PSMA), but also introns and flanking regions of selected genes, including *TP53*, *PTEN*, *RB1*, *FOXA1*, *CHD1*, *MYC*, *AR*, *BRCA2*, *MSH2*, *MSH6* and others. The KAPA HyperChoice MAX 3 Mb T3 panel (Kapa; cat. no. 09052917001) was added at one-third the concentration of the targeted probe set, providing a genome-wide backbone of ~9,000 additional probes (spaced ~350 Kb apart) capturing heterozygous germline single nucleotide polymorphisms (SNPs) at common frequencies across various ancestral backgrounds. This whole-genome backbone approach (median 603× coverage for the cfDNA samples) provides greater resolution to inform on overall genomic instability, assists in differentiating between focal and broad chromosome arm copy number calls, and aids in ctDNA% estimation (see 'Estimation of circulating tumor DNA fraction'). Final libraries were purified with KAPA HyperPure Beads (Kapa; cat. no. 08963843001) before quantification with the Quantus Fluorometer. Library pools were then sequenced on a NovaSeq 6000 S4.

Sequencing alignment and quality control. Following sequencing on Illumina machines, adapters from the 3′-end were trimmed using cutadapt v.4.9 (ref. 74) in paired mode. Low-quality read tails (smoothed base quality <30) were trimmed using an in-house algorithm. Per-base read coverages in target regions were quantified using seqkit v.0.8.1 (https://github.com/annalam/seqkit), after duplicate removal. Paired-end reads were aligned to the hg38 reference genome using Bowtie-2.3.0 (ref. 75). An additional local realignment step was performed using ABRA2 v.2.24 with default parameters, but allowing low mapping quality reads (mapq ≥2) to be included in the realignment to boost insertion and deletion (indel) detection[76]. Duplicate reads were marked using samblaster v.0.1.24 (ref. 77). Germline SNPs were used to verify the patient identity of baseline and progression cfDNA samples and matched WBC.

Somatic mutation identification. Somatic mutations (single nucleotide variants (SNVs) and small indels) were identified from cfDNA as previously described[23–25]. Briefly, independently identified mutations required a minimum supporting mutant read count of ≥8 for coding and ≥20 for noncoding mutations, plus a VAF of ≥1% (reduced to 0.5% for established hotspot mutations). Our minimum required mutant read support equates to an approximate minimum VAF of ~0.5–1% (given our target per-sample depth of 1,500× and expectation of spatial read-coverage stochasticity) aligning with the limits of detection of contemporary commercial pan-cancer ctDNA genotyping companion diagnostics[48]. Note that a minimum VAF of ~0.5–1% mathematically equates to a ctDNA fraction of approximately 2%, below which somatic SNVs or indels are generally not reliably detectable (high false-negative rate) because of the likelihood of insufficient mutant read-support. In addition, we required: (1) ≥20 position-matched read depth in the patient-matched WBC DNA, (2) cfDNA VAF ≥3× and ≥5× higher than the position-matched VAF in the paired WBC DNA for coding and noncoding mutations respectively, and (3) cfDNA VAF to be ≥20× and ≥50× higher than the average position-matched VAF across all WBC DNA samples for coding and noncoding mutations respectively. Per-patient comparison with matched WBC enabled removal of clonal hematopoiesis variants and germline polymorphisms that may masquerade as tumor-derived cfDNA variants in assays that do not perform synchronous WBC sequencing. For base substitutions, the average mapping quality of mutation-supporting reads was required to be ≥10 or ≥30, and the average distance of the mutant allele from the nearest read end must have been ≥15 or ≥25 bases for coding and noncoding mutations, respectively. Protein-level consequences of variants were predicted using ANNOVAR[78]. Additional dependent mutation calling (enabling more sensitive variant detection using a priori information across same-patient serial cfDNA) was adopted to assist with estimating ctDNA% and characterizing treatment-emergent resistance mutations. To call a mutation that had already been independently identified in another same-patient sample, the aforementioned independent mutation calling thresholds were relaxed to ≥3 supporting reads and a VAF of ≥1%. All somatic mutations were manually inspected using Integrated Genomics Viewer.

Germline mutation identification. Germline variants were identified by searching WBC samples for variants with an alternative allele frequency of ≥15% with ≥5 supporting reads. Common germline variants with a population allele frequency of ≥0.5% in GNOMAD were deemed unlikely to be pathogenic or clinically relevant and were discarded. Protein-level consequences of variants were predicted based on ANNOVAR[78]. Variants were considered pathogenic if they resulted in a truncated protein (for example, stopgains, frameshifts) or were missense mutations classified as 'pathogenic' or 'likely pathogenic' based on ClinVar annotation[79].

Copy number alteration analysis. Copy number analysis was performed using previously described custom methodology[12,21]. We leveraged our targeted panel's genome-wide backbone of heterozygous germline SNPs (offering both positional coverage log ratio (LR) information and heterozygous SNP allele frequency (HSAF) data) to fit individual ploidy models to each cfDNA sample, thereby ascertaining chromosomal arm-level copy number alterations, WGD status and ctDNA%. Low ctDNA% fraction (<20%) precludes accurate model fitting and therefore WGD status was considered unevaluable for these cases ('Estimation of circulating tumor DNA fraction' below). All models were manually reviewed. For focal (gene-level) copy number alterations, dense probe coverage in exons and select introns of targeted panel genes facilitated calculation of intragenic median coverage LR and HSAF. Coverage LR is calculated across tumor-normal pairs at base pair resolution, and normalized by median sequencing depth and guanine–cytosine (GC) content. A pool of control cfDNA samples from prostate cancer patients ($n = 31$) with no detectable somatic mutations or copy number alterations (putatively ctDNA-negative) served as a reference for GC correction. For targeted panel genes, LR and HSAF thresholds were used to assign categorical copy number status: (1) deep deletion, LR [-inf, −1]; (2) shallow deletion, LR [−1, −0.3] OR LR [−0.3, −0.15] plus HSAF ≥ 0.6; (3) copy gain, LR [0.3, 0.7] OR LR [0.15, 0.3] plus HSAF ≥ 0.6; (4) amplification, LR [0.7, inf]; and (5) no evidence of copy number alteration. These thresholds were empirically determined by examining the distribution of LR and HSAF in negative control cfDNA samples from healthy volunteers and prostate cancer

patients without detected ctDNA, as previously described[24]. For key clinically relevant genes, absolute copy number calls were manually assessed by comparing gene-level traces of LR and HSAF against each sample's fitted whole-genome ploidy models, allowing a more precise and accurate assessment of allelic configuration and null status ('Biomarker assignment' below).

Identification of structural variants. Structural variants in cfDNA were identified using split-read methodology implemented in the previously validated Breakfast software v.0.6 (github.com/annalam/breakfast) with the--max-frag-len=1000--anchor-len=30--merge-duplicates options. A detailed description of Breakfast and its validation are given in refs. 12,23. A minimum of four unique junction-spanning reads were required to detect a structural variant. Because breakpoint positions of genuine somatic structural variants are almost always unique per-patient tumor, we removed structural variants with identical breakpoints in either the patient's matched WBC or cfDNA samples from any other patient reasoning that these are likely false positives. Structural variants in key prostate cancer driver genes (including *PTEN*, *TP53*, *RB1*, *BRCA1/2*, *ATM* and select DDR-related genes) were manually reviewed for predicted protein impact using UCSC BLAT (https://genome.ucsc.edu/cgi-bin/hgBlat). Any candidate structural rearrangements with supporting split-reads that mapped ambiguously to multiple highly homologous regions were discarded. Only structural variants predicted to disrupt ≥1 exon, or in the case of *AR* presumed to truncate the *AR* LBD, were considered pathogenic and were included in correlative analyses.

Estimation of ctDNA fraction. The ctDNA% for each plasma cfDNA sample was determined using one of two orthogonal approaches: (1) a mutation-based method using the maximal allele frequency of eligible autosomal somatic mutations, or (2) a copy number-based method using genome-wide coverage data and germline heterozygous SNP allele frequencies to fit per-sample ploidy models. Both approaches follow published methodology[12,21,23], and are described below. Note that our two-pronged approach for measuring ctDNA fraction mirrors the contemporary industry-standard methodology utilized by several widely available commercial companion diagnostics. These commercial assays harbor a similar ctDNA fraction limit of detection of ~1–2% (ref. 48), but may be slightly more prone to false-positive ctDNA estimates because of inadequate removal of clonal hematopoiesis through not incorporating synchronous WBC profiling (in contrast to our research assay).

For the mutation-based method, ctDNA% was estimated using the VAF of autosomal somatic mutations in nonamplified genes (coverage LR <0.3) targeted by our sequencing panel and with ≥30 read depth. Somatic mutation VAFs can be elevated in circumstances of concurrent deletion of the wild-type allele (that is, loss of heterozygosity (LOH)). Given difficulties with reliably detecting LOH at low ctDNA fraction, we conservatively assumed that all somatic mutations may be associated with concomitant LOH. Under this assumption, ctDNA fraction and VAF are related because $\text{ctDNA} \sim \text{fraction} = \frac{2}{(\frac{1}{\text{VAF}}+1)}$. The mutation-based ctDNA% estimate was calculated using the somatic mutation with the highest VAF, based on the assumption that this mutation was most likely to represent a truncal alteration present in a majority of ctDNA-contributing cancer cells. In the few cases in which the only mutation identified in the sample was allosomal, the mutation-based ctDNA% was estimated to be equivalent to the VAF. Germline variants, sequencing and alignment artifacts, and clonal hematopoiesis of indeterminate potential can confound somatic mutation-based estimation of the ctDNA fraction, but are largely eliminated through our parallel deep sequencing of patient-matched WBC DNA and manual curation of mutations. For our copy number-based ctDNA fraction estimation strategy, we fit ploidy models to each cfDNA sample's genome-wide coverage LR and HSAF data enabled by the genome-wide SNP grid embedded in our panel. Automated maximum-likelihood solutions were manually vetted and adjusted as necessary to arrive at a final ploidy model for subsequent derivation of segmental copy number status and sample ctDNA%. Acknowledging that copy number-based model fitting accuracy decreases in samples with legitimately low ctDNA%, we used copy number-based ctDNA% estimates for samples with ctDNA ≥20%, and instead leveraged our mutation-based ctDNA% estimates for samples with ctDNA <20% (as assessed via the copy number method). In the event that only an *AR* amplification, structural variant or isolated somatic chromosomal arm aneuploidy was detected in cfDNA without any additional somatic mutations, ctDNA% was conservatively heuristically estimated to be 5%. Samples without detected mutations or focal or large-scale copy number events were categorized as ctDNA-negative. ctDNA% prognostic risk categories of high (30–100%), low (2–30%) and undetectable (<2%) were predefined[20]. Category thresholds were originally heuristically defined to achieve an approximately balanced dichotomization of patients commencing first-line mCRPC therapy in an earlier clinical trial cohort[24]. The lower ctDNA% boundary of 2% corresponds to our targeted assay's approximate lower VAF limit of detection of ~0.5% for somatic SNVs and/or indels.

Biomarker assignment. We used a two-tiered hypothesis testing strategy for all genomic correlative outcomes assessments: first testing binary alteration presence or absence (of any pathogenic defect, excluding monoallelic deletions), then stratifying by compound alteration status, recognizing that (1) distinct classes of genomic alteration may differentially impact protein function and (2) in the context of gene dosage and haploinsufficiency, a significant reduction (beyond that of one-allele loss) or complete loss of functional gene copies may be required to effect a biological or clinical phenotype.

For all clinical correlative analyses, we utilized a set of gene-specific criteria for binarizing patients by presumed pathogenic alteration status (summarized in Supplementary Table 5). This incorporated homozygous deletions of the entire gene body, *AR* genomic structural rearrangements, and SNVs and indels with ≥1% VAF aligning with our previous clinical correlative work[21,24,36], while additionally including non-*AR* structural variants and focal intragenic deletions predicted to disrupt ≥1 exon. Focal intragenic deletions were evaluated by plotting each per-gene LR and HSAF spatial profile with overlaid global ploidy states inferred from genome-wide copy number model fitting, thereby enabling manual validation of our automated per-gene copy number calls, while also identifying focal intragenic events that would be obfuscated by gene-level summary metrics of coverage LR and HSAF (that is, analyzing the gene body as a single unit). Using this information, we enumerated the number of remaining copy-unaltered alleles. Copy status was assumed to be neutral in cases with low ctDNA%, ambiguous or undeterminable ploidy model fitting, or excessive sample sequencing noise and coverage stochasticity (for example, because of GC bias). Monoallelic deletions (either whole-gene or intragenic focal deletions) without any concomitant mutations or structural variants in the same gene were not considered pathogenic—only homozygous deletions of ≥1 exon supported by heterozygous SNP evidence where available were considered as 'alteration present'.

The granular copy number analysis above was synthesized with mutation (both somatic and germline) and structural variant calls to assess the compound alteration status of key genes. We define 'null status' in which all copies of the gene were disrupted and no wild-type copies remain. A gene was considered null if any of the following were true: (1) any coding region of the gene had an absolute copy number of zero (all alleles spanning an exon were deleted); (2) presence of a pathogenic mutation with ≥1% VAF plus LOH, such that all remaining alleles (1 for diploid or 2 for WGD) are mutated and from the same parental origin; (3) presence of a pathogenic mutation with ≥1% VAF plus copy-neutral LOH, such that the wild-type allele was deleted and the

mutated allele was gained and all remaining alleles are mutated (2 for diploid and 4 for WGD); (4) presence of a pathogenic structural variant plus deletion of the wild-type allele; and (5) a combination of multiple structural variants and mutations with ≥1% VAF, which were assumed to affect different alleles unless the alterations were in close enough proximity to be phased. The compound gene status for key genes was critically reviewed by three genomic scientists to reach consensus.

AR gene dosage may differentially influence mCRPC biology and clinical outcomes. Therefore, we focused on two distinct biological categorizations of absolute *AR* copy number (gain versus amplification) for baseline correlative biomarker assessment: (1) *AR* gain, absolute ctDNA fraction adjusted copy number ≥4; and (2) *AR* amplification, absolute ctDNA fraction adjusted copy number ≥8. These definitional thresholds of 4 and 8 correspond roughly to the first and third quartile of absolute *AR* copy number as evaluated in all TheraP baseline ctDNA samples with ctDNA ≥5%. Note that in contrast to SNVs or indels, we only evaluated absolute AR copy number in samples with ctDNA ≥5%. The asymptotic nature of the formula for deriving absolute AR copy number $(1+\frac{2^{(L-d)}-1}{\text{ctDNA\%}}$, where L is the gene LR and d is the diploid level (parameterization of global ploidy fit)) means that the output is highly sensitive to small perturbations or uncertainty in ctDNA fraction, especially in the limit of lower ctDNA%. Therefore, we conservatively heuristically raised the minimum ctDNA fraction to 5% to mitigate inflated error in inferred absolute AR copy number. Across the entire TheraP baseline population, 32 samples had ctDNA ≥2% versus 43 harboring ctDNA ≥5%, and we rationalized that the significant increase in analytical and/or technical stringency outweighed the slight reduction in sample size and statistical power, in electing to use a minimum 5% cutoff for absolute AR copy number assessment.

Assessment of ctDNA population shift

Mutation analysis. In this analysis, we considered only mutations (SNVs and small indels) that were amenable to detection in both timepoints. This includes mutations either already called in both timepoints, or called in only one timepoint and that had a ≥0.9 probability of detecting ≥3 more supporting mutant reads in the other timepoint, assuming that the biological ground-truth VAF did not change across timepoints. This removes mutations that seem to appear or disappear in progression because of variable ctDNA% and/or sequencing depth across timepoints rather than a true CCF change. For example, for a mutation called at baseline and not at progression, $\text{Expected VAF at progression} = \frac{\text{Baseline VAF}\times\text{Progression ctDNA\%}}{\text{Baseline ctDNA\%}}$. The probability of detecting ≥3 supporting reads can then be modeled with $1-F(k,n,p)$ where F is the cumulative distribution function of a binomial distribution with parameters $k=2$, n, which is the mutation location read depth at progression, and p, which is the expected VAF at progression. If the resulting probability is <0.9, then the mutation was excluded from this analysis. The identical (but reciprocal) calculation was performed for mutations called at progression but not at baseline.

To identify likely mutational profile shifts, two lines of evidence were considered: (1) mutations that were called in one timepoint and had zero mutant read support in the other timepoint (that is, newly appeared or disappeared in progression); and (2) mutations that were detected in both timepoints but underwent a significant CCF change. We classified a patient as having a mutational profile shift if they had any of: (1) ≥4 mutations with significant CCF change; (2) ≥1 mutation with CCF change and ≥1 newly appeared or disappeared mutation; or (3) ≥2 newly appeared or disappeared mutations.

Significant CCF change was determined per mutation by first calculating the CCF of the mutation at both timepoints: we calculated the range of VAFs that correspond to CCFs from 0 to 1 at intervals of 0.01, using the sample's ctDNA% and absolute copy number of the mutated gene. For each possible VAF, we then calculated the probability of obtaining the observed number of supporting mutant reads given the read depth at the position, modeled on a binomial distribution. If a mutation had no supporting reads (was undetected in the timepoint), the number of supporting reads was artificially conservatively set to 1 to satisfy Cromwell's rule. In subsequent analyses, the CCF of mutations with no supporting reads were reset to 0. The list of probabilities was normalized against the total cumulative distribution function probability over the range, and the CCF corresponding to the VAF with the maximum posterior probability was taken as the CCF for the mutation. CCFs corresponding to a cumulative probability of 0.025 and 0.975 were taken as the 95% CI. In cases in which the observed VAF implied a CCF beyond the [0, 1] range—common in cases of (copy-neutral) LOH in which only the mutant allele remains—and the list of probabilities in CCF∈[0,1] was 0, the CCF was set to 1. Conservatively, a significant CCF change was called only if the confidence intervals of the mutation CCFs in the two timepoints were separated by ≥0.05.

AR copy number analysis. To evaluate whether serial same-patient differences in absolute *AR* copy number were consistent with a genuine biological shift (versus originating predominately from stochastic technical factors), we performed 10,000 rounds of simulation per sample. Each simulation perturbed the measured intragenic *AR* log ratio and sample ctDNA% with random noise to account for experimental uncertainty. Specifically, ctDNA% (denoted F) was perturbed using both multiplicative and additive Gaussian noise: $F_{\text{sim}} = F_{\text{measured}} \times 2^{N(0,\,\sigma 1)} + N(0,\,\sigma 2)$. Standard deviations $\sigma 1 = 0.12$ and $\sigma 2 = 0.06$ were empirically derived from earlier error modeling of our mutation-based ctDNA% estimation methodology, using matched whole-exome sequencing as the ground truth (as previously described)[23]. To accommodate the orthogonal approaches to measuring ctDNA% used in TheraP ('Estimation of circulating tumor DNA fraction'), we heuristically divided these dispersion parameters σ1 and σ2 by three for samples in which ctDNA% was inferred from the more accurate ploidy-based approach (that is, in samples with true ctDNA% above 20%). Similarly, the measured *AR* log ratio was perturbed by Gaussian noise with a standard deviation of 0.137 (denoted as LR_{sim}). The simulated absolute *AR* copy number for each sample was then computed using $AR_{\text{sim}} = 1 + (\frac{2^{(LR_{\text{sim}}-d)}-1}{(F_{\text{sim}})})$ and stored as a vector up to 10,000 values (simulation rounds where F_{sim} was <2% were discarded to align with our approximate ctDNA% limit of detection and avoid asymptotic behavior in the resultant simulated *AR* copy number distribution). d represents a parameterization of our ploidy model fitting signifying the log ratio representing a diploid state. These AR_{sim} values were sorted, and an 85% CI was empirically calculated and recentered on the sample's true measured absolute *AR* copy number. We considered any pair of matched baseline-progression cfDNA samples to harbor a statistically significant difference in absolute *AR* copy number if their respective 85% CIs did not overlap.

Genome-wide copy number analysis. To robustly detect absolute changes from baseline to progression in copy number status and HSAF detected by whole-genome SNP sequencing, we only leveraged patients with ≥20% ctDNA at both timepoints. Two patients with ≥20% ctDNA were excluded from this analysis because of high sequencing noise in one or both samples from the patient. Using an in-house segmentation algorithm, we aligned segmentation of the whole-genome data of all cfDNA samples (the whole genome was divided in the same bins for every sample). This enabled comparison of copy number status and HSAF across patients and timepoints. Absolute copy number per segment was calculated as $\text{Absolute copy number of the segment} = \frac{(2^{(\text{lr}+1-\text{dl})}-2)}{\text{ctDNAfraction}+2}$. In this formula, lr is the log ratio of the segment from targeted copy number data and dl is the diploid line of the ploidy model of the sample. For the tumor-specific HSAF the following formula was used: $\text{Tumor} \sim \text{HSAF} = \frac{(\text{HSAF}-0.5\times\text{normal}\sim\text{cell}\sim\text{fraction})}{\text{ctDNAfraction}}$. To stringently detect changes

in copy number status and HSAF status, confidence intervals were calculated for every segment using the per segment standard deviation of the log ratio and HSAF. Changes were considered significant if the confidence intervals at baseline and progression did not overlap. Only segments composed of three or more target probes, or three or more heterozygous SNPs were included to evaluate genomic changes in copy number status and HSAF status, respectively. Participants with five or more segments showing either a significant change in copy number status or HSAF status were considered to be patients with whole-genome evidence of a population shift.

Reporting summary

Further information on research design is available in the Nature Portfolio Reporting Summary linked to this article.

Data availability

The hg38 human reference genome was downloaded from UCSC. Germline variant population frequency is available at gnomAD v.3.0 (https://gnomad.broadinstitute.org/). ANZUP is obligated to protect the rights and privacy of trial participants, thereby necessitating restricted access to patient-level clinical and genomic sequencing data. Deidentified participant sequencing and select clinical data will be made available to researchers who are registered with an appropriate institution following publication. Methodologically sound proposals for any purpose will be considered by the trial executive committee who will have the right to review and comment on any draft manuscripts before publication. Proposals should be directed to michael.hofman@petermac.org. To gain access, data requesters will be required to sign a data access agreement. Timeframe for data access will be subject to ANZUP policy and process. Data supporting the findings of this study are available in the article in Supplementary Tables 1–11. Source data are provided with this paper.

Code availability

Our complete ctDNA somatic variant calling pipeline is available on GitHub (https://github.com/annalam/cfdna-wgs-manuscript-code) and is described in detail in a previous publication[12]. No additional custom software was utilized for any analysis performed herein.

References

73. Hofman, M. S. et al. TheraP: a randomized phase 2 trial of ^{177}Lu-PSMA-617 theranostic treatment vs cabazitaxel in progressive metastatic castration-resistant prostate cancer (Clinical Trial Protocol ANZUP 1603). *BJU Int.* **124**, 5–13 (2019).
74. Martin, M. Cutadapt removes adapter sequences from high-throughput sequencing reads. *EMBnet J.* **17**, 10–12 (2011).
75. Langmead, B. & Salzberg, S. L. Fast gapped-read alignment with Bowtie 2. *Nat. Methods* **9**, 357–359 (2012).
76. Mose, L. E., Perou, C. M. & Parker, J. S. Improved indel detection in DNA and RNA via realignment with ABRA2. *Bioinformatics* **35**, 2966–2973 (2019).
77. Faust, G. G. & Hall, I. M. SAMBLASTER: fast duplicate marking and structural variant read extraction. *Bioinformatics* **30**, 2503–2505 (2014).
78. Wang, K., Li, M. & Hakonarson, H. ANNOVAR: functional annotation of genetic variants from high-throughput sequencing data. *Nucleic Acids Res.* **38**, e164 (2010).
79. Landrum, M. J. et al. ClinVar: improving access to variant interpretations and supporting evidence. *Nucleic Acids Res.* **46**, D1062–D1067 (2018).

Acknowledgements

The TheraP trial (ANZUP 1603) is a collaboration between the ANZUP Trials Group, the NHMRC Clinical Trials Centre, University of Sydney and the Australasian Radiopharmaceutical Trials Network (ARTnet) in partnership with the Prostate Cancer Foundation of Australia with support from ANSTO, Endocyte (a Novartis company), Movember, The Distinguished Gentleman's Ride, It's a Bloke Thing and CAN4CANCER. ANZUP receives infrastructure support from the Australian government through Cancer Australia (Support for Cancer Clinical Trials Program). This correlative research study was primarily supported by the Prostate Cancer Foundation via a 2023 PCF Challenge Award to A.W.W. Additional funding support was also received from a Terry Fox New Frontiers Program Project Grant and a Canadian Cancer Society Challenge Grant (grant no. 707339). E.M.K. is supported by a Prostate Cancer Foundation Young Investigator Award and an ANZUP Synchrony Fellowship. S.H.T. is supported by a Prostate Cancer Foundation Young Investigator Award and Michael Smith Health Research BC Trainee Award. J.P.B. is supported by a Prostate Cancer Foundation Young Investigator Award and PhD support through an Australian Government Research Training Program Scholarship. A.M.S. was supported by an NHMRC Investigator Fellowship (APP1177837). I.D.D. is supported by an NHMRC Practitioner Fellowship (APP1102604). M.S.H. acknowledges philanthropic and government grant support from the Prostate Cancer Foundation, the Peter MacCallum Foundation and a NHMRC Investigator Grant and Movember. S.S. is supported by the NHMRC and additionally acknowledges grant support from the Prostate Cancer Foundation and the Peter MacCallum Foundation. The NHMRC Clinical Trials Centre was supported by NHMRC Program Grants 1037786 and 1150467. ^{177}Lu was supplied by ANSTO. Endocyte provided PSMA-11 and PSMA-617, and additional funding support. We acknowledge and thank the 200 patients for their participation in the TheraP study; and the principal investigators, coinvestigators, study coordinators, nurses, radiopharmacists and chemists and nuclear medicine technologists at the 11 centers across Australia for their dedication and enthusiasm. We also thank members and staff of the ANZUP Board, Scientific Advisory Committee, Prostate Cancer Subcommittee, Consumer Advisory Panel and Independent Data Safety and Monitoring Committee; NHMRC Clinical Trials Centre; and ARTnet.

Author contributions

Conceptualization: E.M.K., L.E., A.J.M., I.D.D., M.S.H., A.A.A. and A.W.W. Methodology: E.M.K., S.W.S.N., S.H.T., M.A., C.H. and A.W.W. Software: E.M.K., S.W.S.N., S.H.T., M.A., C.H. and A.W.W. Validation: E.M.K., S.W.S.N., S.H.T., C.H. and A.W.W. Formal analysis: E.M.K., S.W.S.N., S.H.T., M.A., C.H. and A.W.W. Investigation: E.M.K., S.W.S.N., S.H.T., G.D., C.H. and A.W.W. Resources: M.A., I.D.D., M.S.H., A.A.A. and A.W.W. Data curation: E.M.K., S.W.S.N., S.H.T., S.S., G.D., C.H. and A.W.W. Writing—original draft: E.M.K., S.W.S.N., S.H.T., C.H. and A.W.W. Writing—review and editing: E.M.K., S.W.S.N., S.H.T., L.E., S.S., J.P.B., A.I., A.M.J., R.J.F., V.S., S.-T.L., A.M.S., A.J.M., M.R.S., M.A., C.H., I.D.D., M.S.H., A.A.A. and A.W.W. Visualization: E.M.K., S.W.S.N., S.H.T., C.H. and A.W.W. Supervision: I.D.D., M.S.H., A.A.A. and A.W.W. Project administration: E.M.K. V.S., I.D.D., M.S.H., A.A.A. and A.W.W. Funding acquisition: I.D.D., M.S.H., A.A.A. and A.W.W.

Competing interests

E.M.K. has consulted or served in an advisory role for Astellas Pharma, Janssen and Ipsen, received travel funding from Astellas Pharma, Pfizer, Ipsen and Roche, received honoraria from Janssen, Ipsen, Astellas Pharma and Research Review, and received research funding from Astellas Pharma (institutional) and AstraZeneca (institutional). L.E. has consulted or served in an advisory role for Noxopharm and Clarity Pharmaceuticals, participated in a speakers' bureau for Janssen Oncology, Mundipharma and Astellas Pharma, and received research funding from Noxopharm (institutional) and Novartis (institutional). S.S. has consulted or served in an advisory role for AstraZeneca, Bristol-Myers Squibb, Merck Sharp & Dohme, Novartis, Skyline Diagnostics and AbbVie, received honoraria from

Bristol-Myers Squibb (institutional), Merck (institutional), AstraZeneca (institutional) and Janssen (institutional), and received research funding from Amgen (institutional), AstraZeneca (institutional), Merck (institutional), Endocyte/Advanced Accelerator Applications (institutional), Roche/Genentech (institutional), Novartis (institutional), Pfizer (institutional) and Senhwa Biosciences (institutional). A.I. has consulted or served in an advisory role for Novartis, Lantheus, Curium, ITM, Bayer, Boston Scientific, Ambrx/J&J (institutional), and received research funding from NIH (institutional), Novartis (institutional), SNMMI (institutional) and ACR (institutional). A.M.J. has consulted or served in an advisory role for Janssen Oncology, Ipsen, AstraZeneca, Sanofi, Pfizer, Novartis, Merck Serono, Eisai, IDEAYA Biosciences, IQvia, Bayer, Astellas Pharma, Grey Wolf Therapeutics, Medison and Starpharma, has a patent or received royalties with Cancer Therapeutic Methods, owns stock or holds ownership interests in Pricilium Therapeutics and Opthea, and receives research funding from Bristol-Myers Squibb (institutional), Janssen Oncology (institutional), Merck Sharpe & Dohme (institutional), Mayna Pharma (institutional), Roche/Genentech (institutional), Bayer (institutional), Lilly (institutional), Pfizer (institutional), AstraZeneca (institutional) and Corvus Pharmaceuticals (institutional). R.J.F. consulted or served in an advisory role for AIQ Solutions, receives research funding from AIQ Solutions, and has an immediate family member employed by and owns stock in AIQ Solutions. A.M.S. has consulted or served in an advisory role for ImmunOs Therapeutics and Imagion Biosystems, has an institutional patent relating to antibodies to EGFR, HER2, PDGF-CC, FN-14, GM-CSF, EphA3, owns stock or holds ownership interests in Paracrine Therapeutics and Certis Therapeutics, and received research funding from Telix Pharmaceuticals (institutional), Curis (institutional), Isotopen Technologien (institutional), Adalta (institutional), Fusion Pharmaceuticals (institutional), AstraZeneca (institutional), EMD Serono (institutional), Cyclotek (institutional), AVID/Lilly (institutional), Merck (institutional), Humanigen (institutional) and Antengene (institutional). M.R.S. has received research funding from Astellas Pharma (institutional), Bayer (institutional), Medivation (institutional), Pfizer (institutional), AstraZeneca (institutional), Bristol-Myers Squibb (institutional), Roche (institutional), Amgen (institutional), Merck Sharpe & Dohme (institutional), Tilray (institutional), BeiGene (institutional) and Novartis (institutional). M.A. is compensated for a leadership role in Fluivia and owns stock in Fluivia. S.H.T. has received honoraria from Bayer. I.D.D. is the unremunerated chair of ANZUP Cancer Trials Group, and has received research funding from Astellas Pharma (institutional), Pfizer (institutional), Roche/Genentech (institutional), MSD Oncology (institutional), AstraZeneca (institutional), Janssen Oncology (institutional), Eisai (institutional), Bayer (institutional), Amgen (institutional), Bristol-Myers Squibb (institutional), Movember Foundation (institutional), Exelixis (institutional), Ipsen (institutional), Seagen (institutional) and ESSA (institutional). M.S.H. has consulted or served in an advisory role for Janssen, MSD and Novartis, received travel funding from Novartis and Debiopharm Group, and received research funding from Bayer (institutional), Novartis (institutional), Isotopia Molecular Imaging (institutional) and Debiopharm Group (institutional). A.A.A. has consulted or served in an advisory role for Astellas Pharma, Novartis, Janssen, Sanofi, AstraZeneca, Pfizer, Bristol-Myers Squibb, Tolmar, Telix Pharmaceuticals, Merck Sharpe & Dohme, Bayer, Ipsen, Merck Serono, Amgen, Noxopharma, Aculeus Therapeutics and Daiichi Sankyo, participated in a speakers' bureau for Astellas Pharma, Novartis, Amgen, Bayer, Janssen, Ipsen, Bristol-Myers Squibb and Merck Serono, received travel funding from Astellas Pharma, Sanofi, Merck Serono, Amgen, Janssen, Tolmar, Pfizer, Bayer and Hinova Pharmaceuticals, received honoraria from Janssen, Astellas Pharma, Novartis, Tolmar, Amgen, Pfizer, Bayer, Telix Pharmaceuticals, Bristol-Myers Squibb, Merck Serono, AstraZeneca, Sanofi, Ipsen, Merck Sharpe & Dohme, Noxopharm, Aculeus Therapeutics and Daiichi Sankyo, and received research funding Astellas Pharma (institutional), Merck Serono (institutional), Novartis (institutional), Pfizer (institutional), Bristol-Myers Squibb (institutional), Sanofi (institutional), AstraZeneca (institutional), GlaxoSmithKline (institutional), Aptevo Therapeutics (institutional), MedImmune (institutional), Bionomics (institutional), Synthorx (institutional), Astellas Pharma (institutional), Ipsen (institutional), Merck Serono (institutional), Lilly (institutional), Gilead Sciences (institutional), Exelixis (institutional), MSD (institutional) and Hinova Pharmaceuticals (institutional). A.W.W. has received honoraria from Janssen, Astellas Pharma, AstraZeneca, Merck, Bayer, Pfizer and EMD Serono, and received research funding from Promontory Therapeutics (institutional), ESSA Pharma (institutional) and Tyra Biosciences (institutional). The other authors declare no competing interests.

Additional information

Extended data is available for this paper at https://doi.org/10.1038/s41591-025-03704-9.

Supplementary information The online version contains supplementary material available at https://doi.org/10.1038/s41591-025-03704-9.

Correspondence and requests for materials should be addressed to Ian D. Davis, Michael S. Hofman, Arun A. Azad or Alexander W. Wyatt.

Peer review information *Nature Medicine* thanks David Miyamoto, Oliver Sartor and the other, anonymous, reviewer(s) for their contribution to the peer review of this work. Primary Handling Editor: Ulrike Harjes, in collaboration with the *Nature Medicine* team.

Reprints and permissions information is available at www.nature.com/reprints.

https://doi.org/10.1038/s41591-025-03704-9

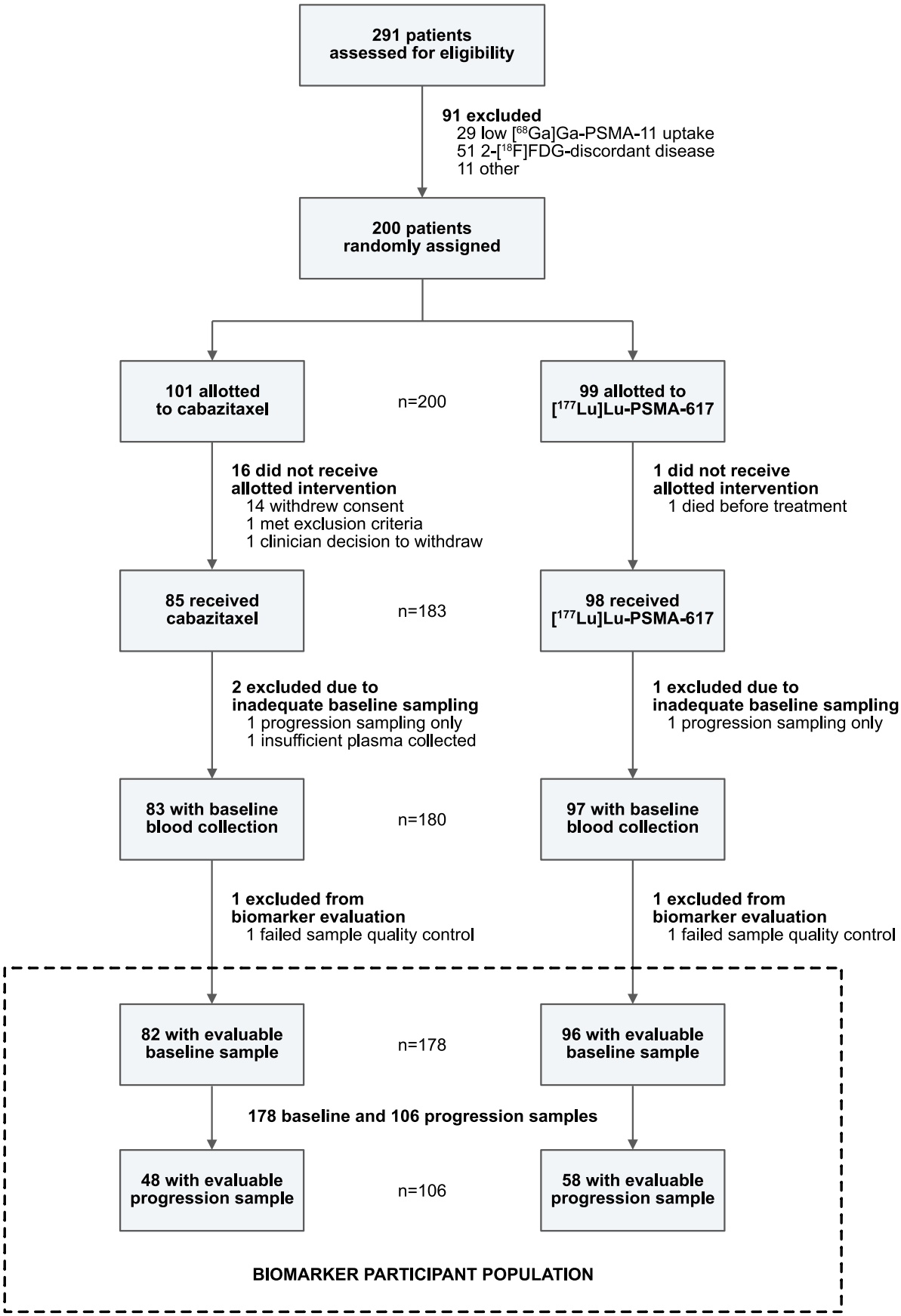

Extended Data Fig. 1 | CONSORT diagram for sequencing and enrolment. CONSORT diagram of participant and sample flow culminating in the formation of the biomarker participant population.

https://doi.org/10.1038/s41591-025-03704-9

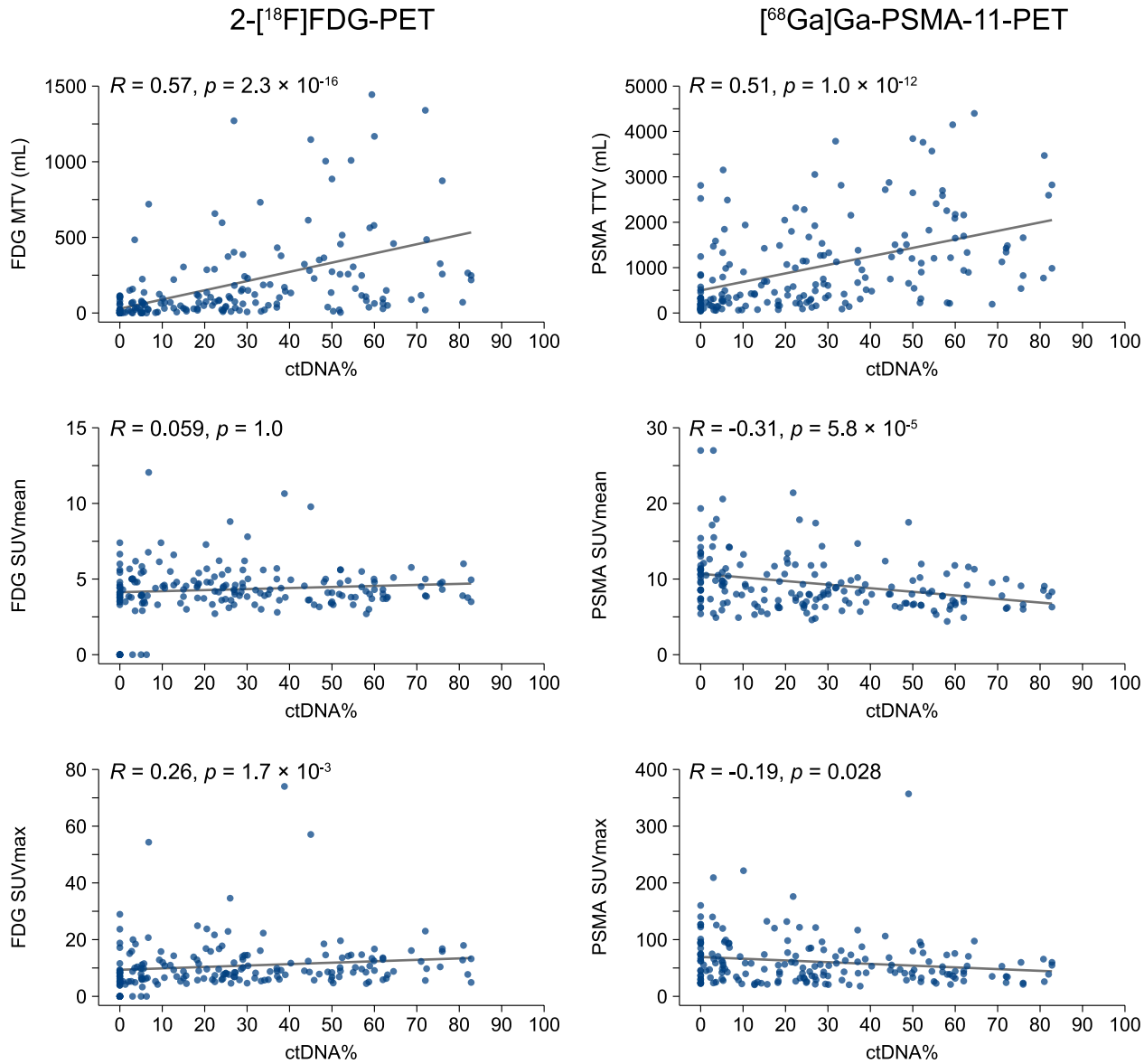

Extended Data Fig. 2 | ctDNA% versus baseline PET imaging variables. Correlation between ctDNA% and four quantitative PET imaging variables. Spearman's rho (two-sided) is reported for each comparison, with p-values adjusted using Bonferroni correction (α = 0.05, m = 3; correcting for three pairwise comparisons within each imaging modality). A grey line represents the linear regression to illustrate the bivariate relationships. FDG, 2-[18F]fluoro-2-deoxy-D-glucose; MTV, metabolic tumour volume; PSMA, prostate-specific membrane antigen; SUV, standardised uptake value.

https://doi.org/10.1038/s41591-025-03704-9

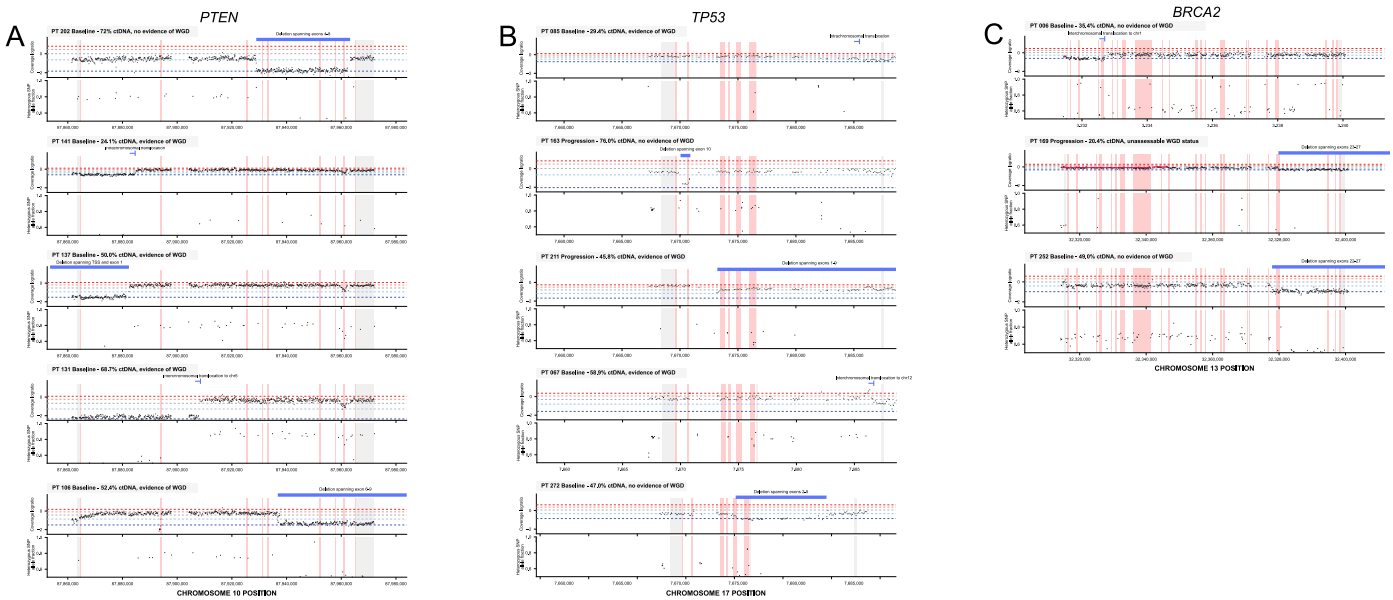

Extended Data Fig. 3 | *PTEN*, *TP53*, and *BRCA2* structural variants. Examples of structural variants and associated focal copy number alterations in (**a**) *PTEN*, (**b**) *TP53*, and (**c**) *BRCA2*. SNP, single nucleotide polymorphism.

https://doi.org/10.1038/s41591-025-03704-9

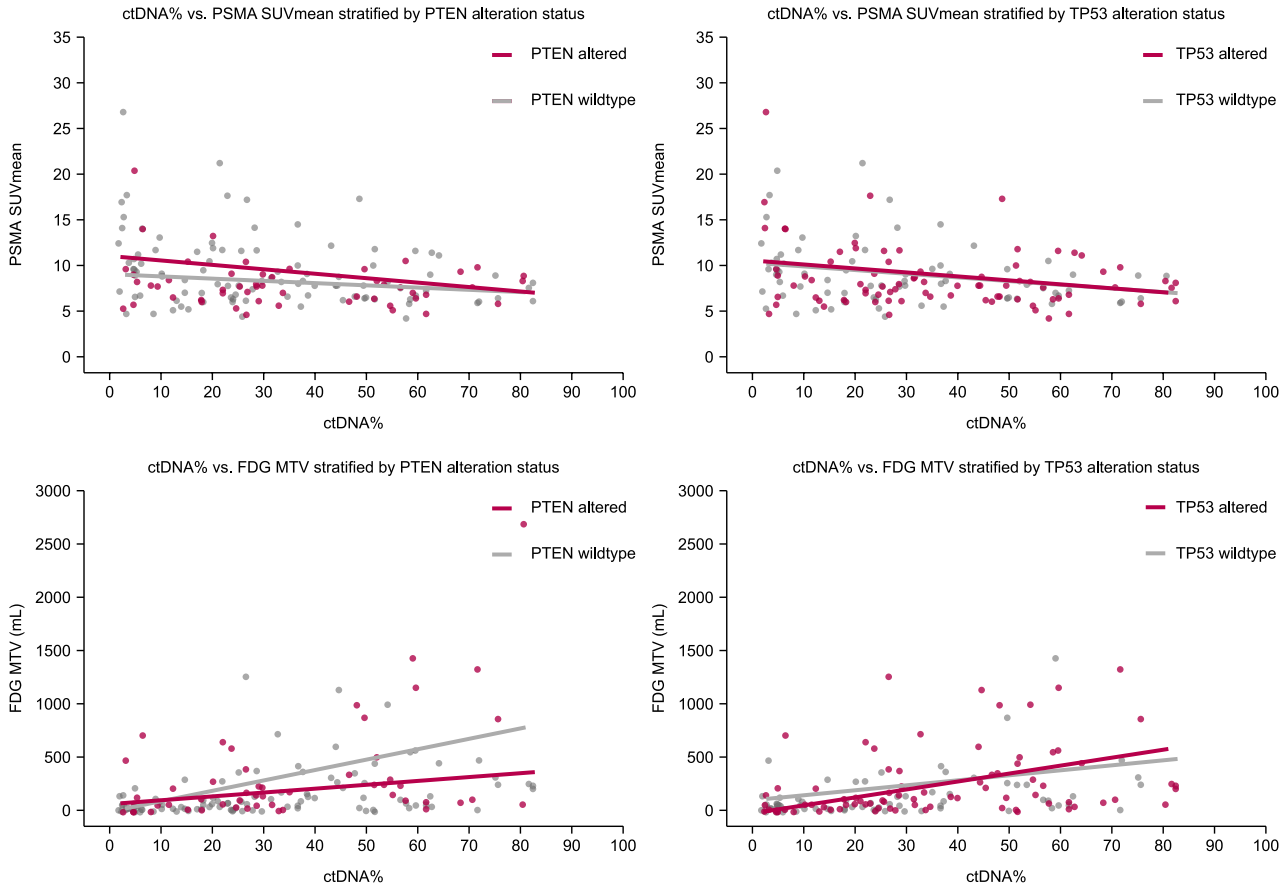

Extended Data Fig. 4 | Relationship between ctDNA% and molecular imaging variables by *PTEN* and *TP53* status. Correlation between ctDNA% and two quantitative PET imaging variables (PSMA SUVmean - top, FDG MTV - bottom), stratified by genomic alteration status (PTEN - left, TP53 - right).

https://doi.org/10.1038/s41591-025-03704-9

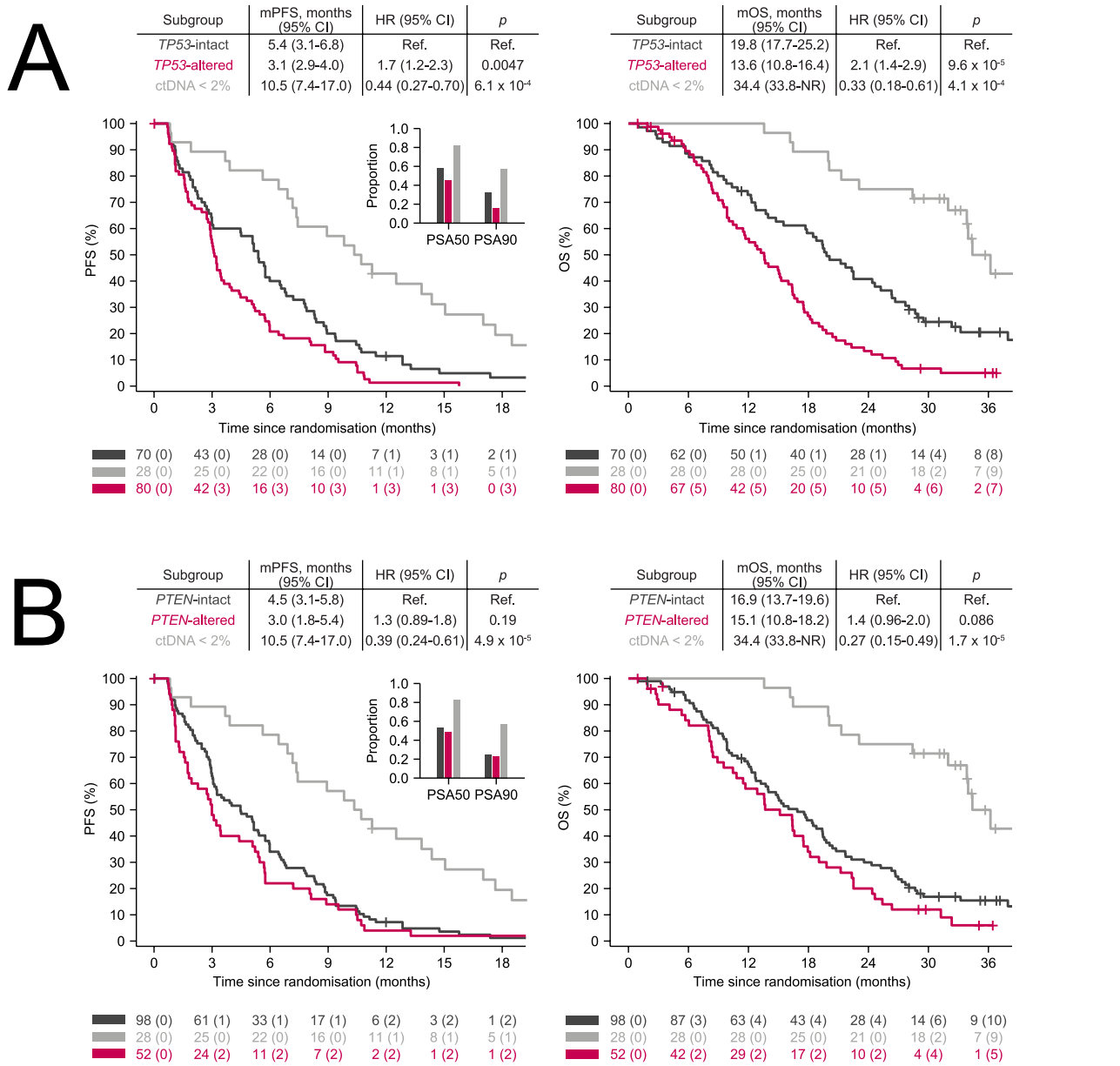

Extended Data Fig. 5 | PFS and OS by *TP53* and *PTEN* alteration status in all-comers. Kaplan-Meier estimates of progression-free survival and overall survival stratified by (**a**) *TP53* alteration status and (**b**) *PTEN* alteration status. Each survival curve includes estimates for three-levels: ctDNA <2%, intact status, and altered status. In-set summary bar plots in the progression-free survival curves represent the proportion of patients that experienced a PSA50 and PSA90 response. An alteration is defined as any mutation(s) or structural variant(s), deep deletion, or expected null gene status. Monoallelic deletions in isolation were not considered altered. In-set tables show univariable hazard ratios from a Cox proportional hazards model. CI, confidence interval; HR, hazard ratio; mPFS, median progression-free survival; NR, not reached; OS, overall survival; PFS, progression-free survival; PSA, prostate-specific antigen; Ref, reference.

https://doi.org/10.1038/s41591-025-03704-9

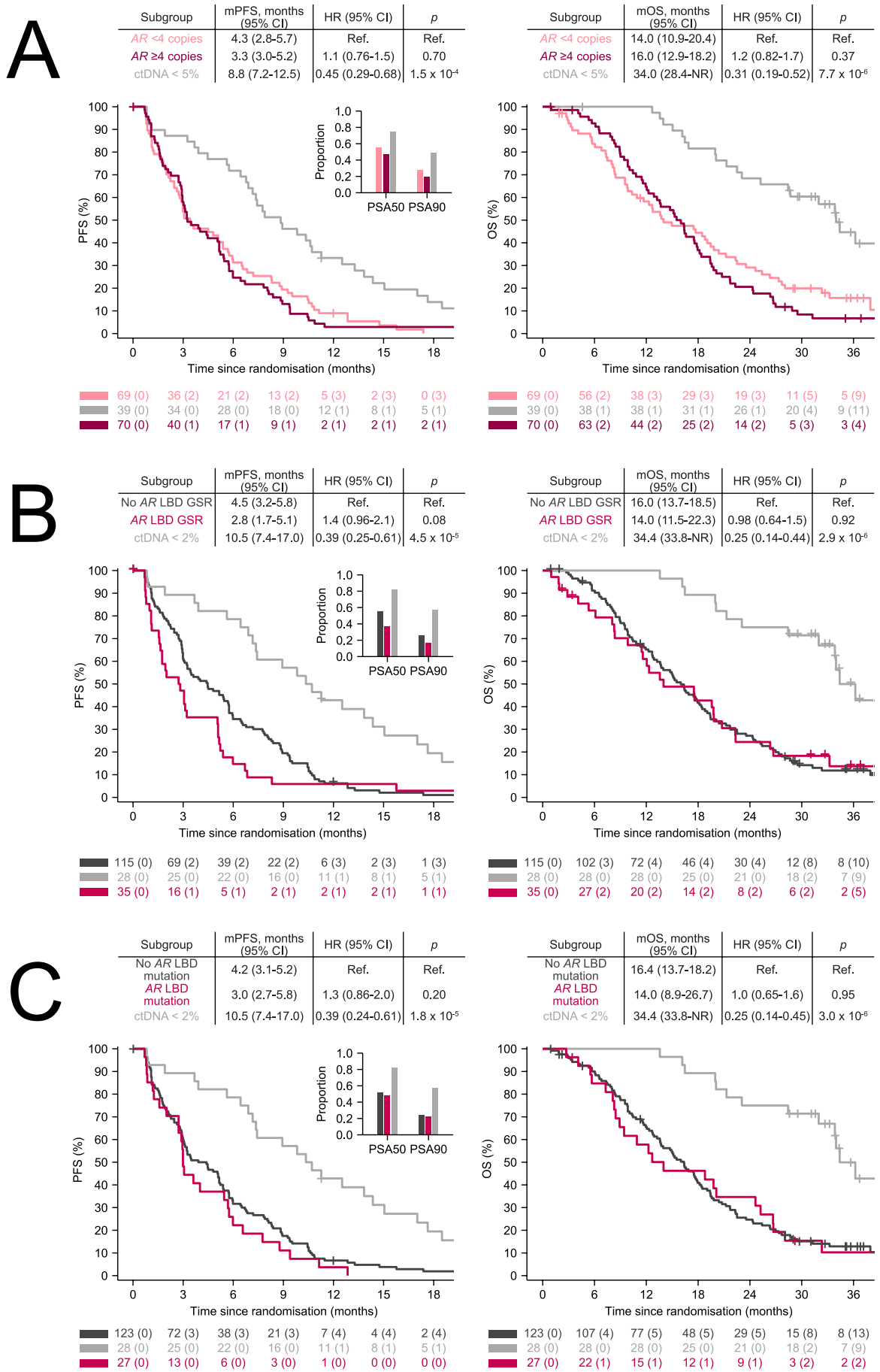

Extended Data Fig. 6 | See next page for caption.

https://doi.org/10.1038/s41591-025-03704-9

Extended Data Fig. 6 | PFS and OS by *AR* alteration status in all-comers. Kaplan-Meier estimates of progression-free survival and overall survival stratified by (**a**) *AR* gain (defined as ≥4 absolute AR copies) status, (**b**) presence of *AR* LBD GSRs, and (**c**) *AR* LBD mutation status. Each survival curve includes estimates for three-levels: ctDNA <2%, intact status, and altered status. In-set summary bar plots in the progression-free survival curves represent the proportion of patients that experienced a PSA50 and PSA90 response. In-set tables show univariable hazard ratios from a Cox proportional hazards model. CI, confidence interval; HR, hazard ratio; GSR, gene structural rearrangement; LBD, ligand binding domain; mPFS, median progression-free survival; NR, not reached; OS, overall survival; PFS, progression-free survival; PSA, prostate-specific antigen; Ref, reference.

https://doi.org/10.1038/s41591-025-03704-9

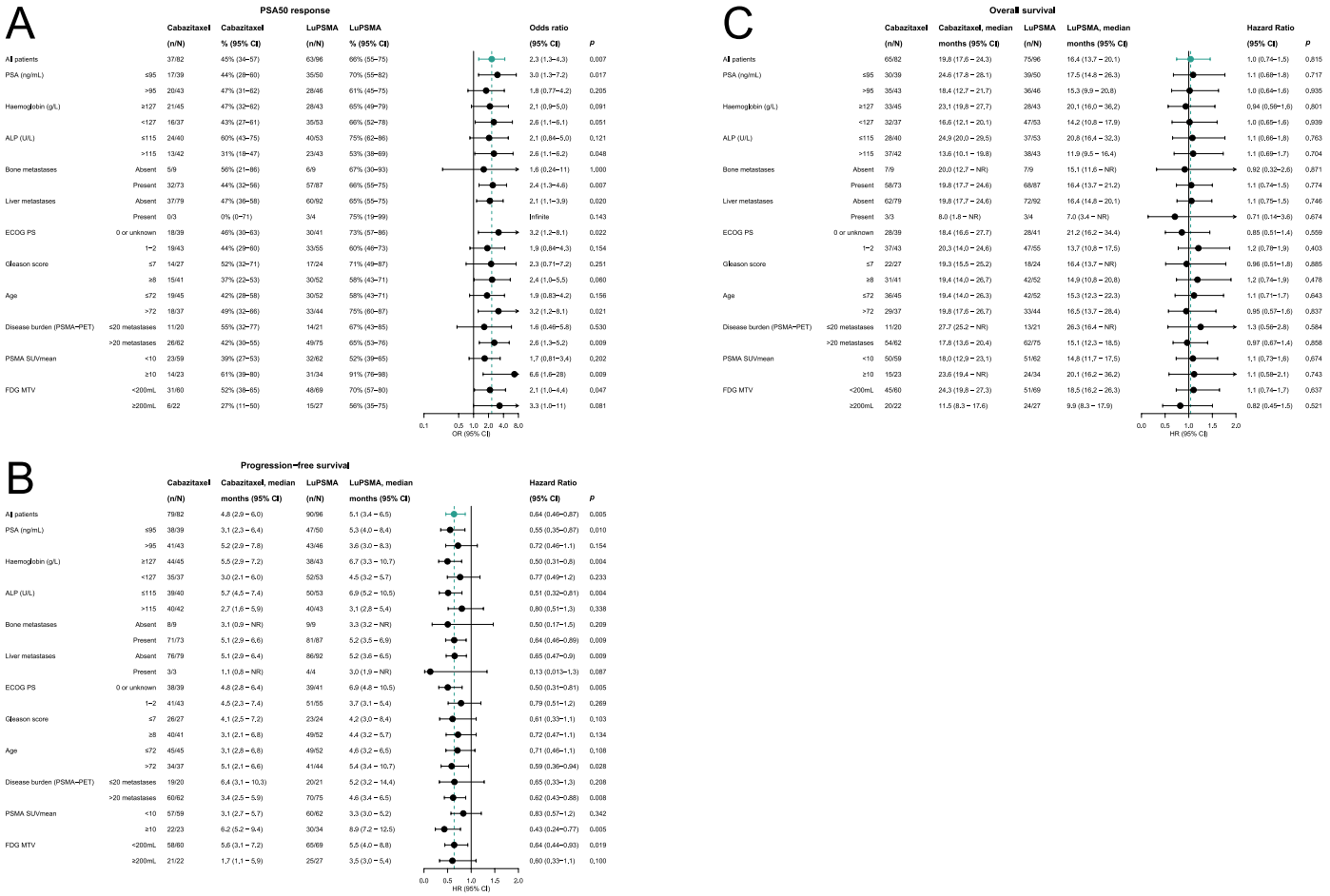

Extended Data Fig. 7 | Clinical outcomes by baseline clinical variables in all-comers. Forest plots show post-hoc sensitivity analyses for (**a**) PSA50 response, (**b**) progression-free survival, and (**c**) overall survival endpoints according to baseline clinical variables. The 'All patients' category includes those in the all-comers biomarker population (n = 178). ALP, alkaline phosphatase; ECOG PS, Eastern Cooperative Oncology Group performance status; FDG, 2-[^{18}F] fluoro-2-deoxy-D-glucose; HR, hazard ratio; MTV, metabolic tumour volume; PSA, prostate-specific antigen; PSMA, prostate-specific membrane antigen; Ref, reference; SUV, standardised uptake value.

https://doi.org/10.1038/s41591-025-03704-9

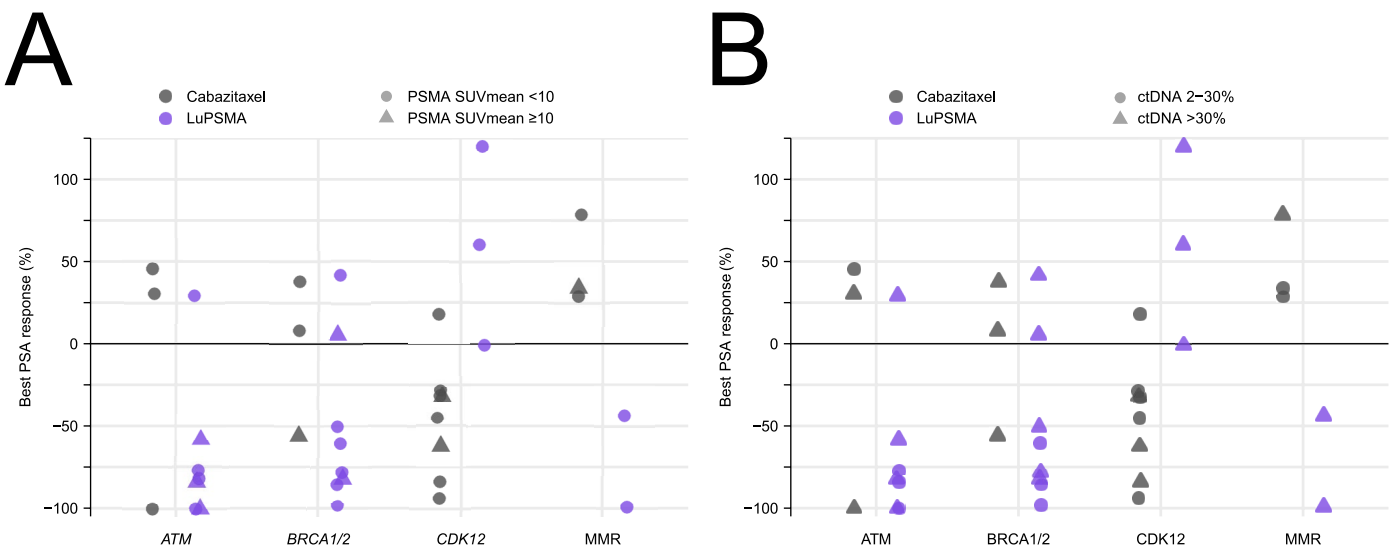

Extended Data Fig. 8 | PSA response by DDR alterations. Best PSA response in the four most commonly altered DNA damage repair-related gene categories: *ATM*, *BRCA1/2*, *CDK12*, and mismatch repair. PSA response for each gene category is expressed at a per-treatment arm level, and further stratified by either (**a**) PSMA SUVmean (<10 and ≥10) or (**b**) ctDNA% level (medium [2–30%] and high [>30%]). MMR, mismatch repair; PSA, prostate-specific antigen; PSMA, prostate-specific membrane antigen; SUV, standardised uptake value.

https://doi.org/10.1038/s41591-025-03704-9

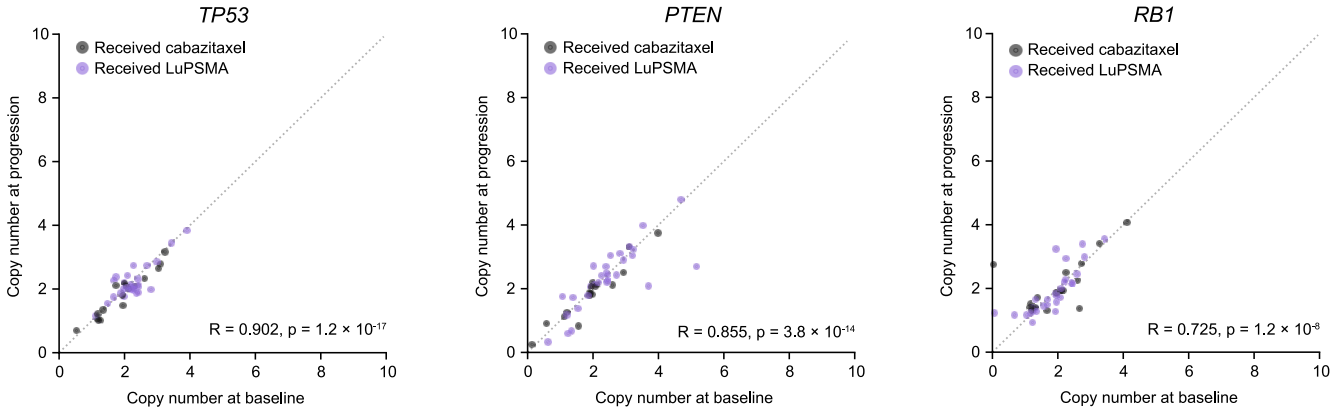

Extended Data Fig. 9 | Copy number status in tumour suppressor genes across consecutive samples. Correlation of the copy number status of tumour suppressor genes *TP53*, *PTEN* and *RB1* between consecutive ctDNA samples from the same patient. Each dot represents a consecutive sample pair (baseline and progression). Pearson's correlation coefficient (two-sided) is reported for each comparison.

nature portfolio

Corresponding author(s): Alexander W. Wyatt

Last updated by author(s): Mar 25, 2025

Reporting Summary

Nature Portfolio wishes to improve the reproducibility of the work that we publish. This form provides structure for consistency and transparency in reporting. For further information on Nature Portfolio policies, see our Editorial Policies and the Editorial Policy Checklist.

Statistics

For all statistical analyses, confirm that the following items are present in the figure legend, table legend, main text, or Methods section.

n/a	Confirmed
☐	☒ The exact sample size (*n*) for each experimental group/condition, given as a discrete number and unit of measurement
☐	☒ A statement on whether measurements were taken from distinct samples or whether the same sample was measured repeatedly
☐	☒ The statistical test(s) used AND whether they are one- or two-sided *Only common tests should be described solely by name; describe more complex techniques in the Methods section.*
☐	☒ A description of all covariates tested
☐	☒ A description of any assumptions or corrections, such as tests of normality and adjustment for multiple comparisons
☐	☒ A full description of the statistical parameters including central tendency (e.g. means) or other basic estimates (e.g. regression coefficient) AND variation (e.g. standard deviation) or associated estimates of uncertainty (e.g. confidence intervals)
☐	☒ For null hypothesis testing, the test statistic (e.g. *F*, *t*, *r*) with confidence intervals, effect sizes, degrees of freedom and *P* value noted *Give P values as exact values whenever suitable.*
☒	☐ For Bayesian analysis, information on the choice of priors and Markov chain Monte Carlo settings
☒	☐ For hierarchical and complex designs, identification of the appropriate level for tests and full reporting of outcomes
☐	☒ Estimates of effect sizes (e.g. Cohen's *d*, Pearson's *r*), indicating how they were calculated

Our web collection on statistics for biologists contains articles on many of the points above.

Software and code

Policy information about availability of computer code

Data collection	No custom software was used to collect data. Blood samples and patient meta data were collected as described in the original clinical trial protocol. Sequencing data was generated and analyzed in-house by co-authors as described in the manuscript Methods and Supplementary Information. Patient clinical data was originally collected and curated/audited as part of the original clinical study publications (Hofman et al., Lancet 2021; Hofman et al., Lancet Oncology 2024).
Data analysis	As described in the Methods, statistical tests and data analyses were conducted in R v.4.4.0 (using dplyr v1.1.4, forcats v1.0.0, janitor 2.2.0, lubridate v1.9.3, purr v1.0.2, psych v2.4.3, stringr v1.5.1, stats v.4.4.0, gtsummary v1.7.2, survival v3.5-8) and in Python 3.9.12 (using pandas v.1.4.2, numpy v.1.23.5, scipy v.1.10.1, statsmodels v.0.13.5), and Julia v1.8.5. Visualisations were generated using the R packages ggplot2 v.3.4.3, forestplot v3.1.3, survminer v.0.4.9, cowplot v.1.1.3, and patchwork v.1.2.0, and the Python packages matplotlib v.3.7.1 and seaborn v.0.13.0. The following bioinformatics/genomic analysis software was used: cutadapt v.4.9, seqkit v.0.8.1, Bowtie2 v.2.3.4.3, samblaster v.0.1.24, bedtools v.2.26, samtools v.1.8 (htslib v.1.8), Mutato v.0.8, and ANNOVAR (v.20191024). Our complete ctDNA somatic variant calling pipeline is available on GitHub (https://github.com/annalam/cfdna-wgs-manuscript-code) and is described in detail in a prior publication(Herberts et al. 2022). No additional custom software was utilised for any analysis performed herein.

For manuscripts utilizing custom algorithms or software that are central to the research but not yet described in published literature, software must be made available to editors and reviewers. We strongly encourage code deposition in a community repository (e.g. GitHub). See the Nature Portfolio guidelines for submitting code & software for further information.

Data

Policy information about availability of data

All manuscripts must include a data availability statement. This statement should provide the following information, where applicable:

- Accession codes, unique identifiers, or web links for publicly available datasets
- A description of any restrictions on data availability
- For clinical datasets or third party data, please ensure that the statement adheres to our policy

ANZUP is obligated to protect the rights and privacy of trial participants, thereby necessitating restricted access to patient-level clinical and genomic sequencing data. De-identified participant data will be made available to researchers who are registered with an appropriate institution following publication. Methodologically sound proposals for any purpose will be considered by the trial executive committee who will have the right to review and comment on any draft manuscripts before publication. Proposals should be directed to michael.hofman@petermac.org. To gain access, data requesters will be required to sign a data access agreement. Timeframe for data access will be subject to ANZUP policy and process. All other data supporting the findings of this study are available within the article (including its Supplementary Data and Source Data files).

Research involving human participants, their data, or biological material

Policy information about studies with human participants or human data. See also policy information about sex, gender (identity/presentation), and sexual orientation and race, ethnicity and racism.

Reporting on sex and gender	Prostate cancer only affects people with prostates (i.e. biological males). This cohort includes people with prostate cancer irrespective of gender identity. All samples are de-identified at time of collection, and all researchers are blind to patient gender identity and gender presentation.
Reporting on race, ethnicity, or other socially relevant groupings	Race and ethnicity data was not provided to researchers conducting this study, and no groupings related to race and ethnicity were used.
Population characteristics	Patient characteristics of the clinical trial have been extensively described in prior publications (Hofman et al., Lancet 2021; Hofman et al., Lancet Oncology 2024), and can also be found in Supplementary Table 1 of this manuscript.
Recruitment	Recruitment details have been comprehensively described in the original trial publications, the ClinicalTrials.gov entry (https://clinicaltrials.gov/study/NCT03392428), and the trial protocol (https://bjui-journals.onlinelibrary.wiley.com/doi/10.1111/bju.14876). We analyzed samples from patients who were enrolled and voluntarily consented to provide samples for research purposes. All participants were screened with [68Ga]Ga-PSMA-11 (PSMA-PET) and 2-[18F]FDG-PET (FDG-PET) scans to select for high PSMA uptake at metastatic site(s) without discordant disease (2-[18F]FDG-positive lesion with low/no PSMA uptake). As described in the manuscript, the biological implications of this stringent imaging pre-selection may limit generalisability of our findings to settings where FDG-PET is not used to evaluate PSMA radioligand therapy candidacy.
Ethics oversight	TheraP was a multicentre trial and received ethics approval at each participating institute. All participants provided signed, written, and informed consent for their samples to be used for research purposes. The trial was done in accordance with the principles of the Good Clinical Practice guidelines and the Declaration of Helsinki.

Note that full information on the approval of the study protocol must also be provided in the manuscript.

Field-specific reporting

Please select the one below that is the best fit for your research. If you are not sure, read the appropriate sections before making your selection.

☒ Life sciences ☐ Behavioural & social sciences ☐ Ecological, evolutionary & environmental sciences

For a reference copy of the document with all sections, see nature.com/documents/nr-reporting-summary-flat.pdf

Life sciences study design

All studies must disclose on these points even when the disclosure is negative.

Sample size	Sample size was not predetermined for this exploratory post hoc analysis - we analyzed all samples from patients enrolled in the trial (NCT03392428, ACTRN12615000912583) who had a baseline sample collected. No formal predefined criteria was used to determine minimum acceptable sample size for exploratory correlative analyses.
Data exclusions	The inclusion criteria for the trial (NCT03392428, ACTRN12615000912583) has been previously published. From the overall cohort, we excluded two patients due to inadequate sequencing data quality of their baseline cfDNA samples. When samples were excluded from sub-analyses, the rationale and denominators are clearly listed in the manuscript text and/or annotated in the figures and figure legends.
Replication	Analyses were descriptive. No experiments requiring technical or biological replicates were performed (as is convention for panel-based DNA

Replication	sequencing of clinical trial samples). Repeat sequencing of identical plasma samples was not performed.
Randomization	Randomization is not used in our descriptive post hoc correlative study, although the original trial (NCT03392428, ACTRN12615000912583) from which samples were obtained is a randomized clinical trial. Randomization is categorically not applicable to any of the descriptive statistical methodology contained herein (e.g. we do not use any complex machine-learning models or bootstrapping methods where random sampling is embedded).
Blinding	The original trial (NCT03392428, ACTRN12615000912583) from which samples were obtained was open-label. Researchers are not blind to patient treatment allocation or clinical characteristics for this post hoc correlative study.

Reporting for specific materials, systems and methods

We require information from authors about some types of materials, experimental systems and methods used in many studies. Here, indicate whether each material, system or method listed is relevant to your study. If you are not sure if a list item applies to your research, read the appropriate section before selecting a response.

Materials & experimental systems

n/a	Involved in the study
☒	☐ Antibodies
☒	☐ Eukaryotic cell lines
☒	☐ Palaeontology and archaeology
☒	☐ Animals and other organisms
☐	☒ Clinical data
☒	☐ Dual use research of concern
☒	☐ Plants

Methods

n/a	Involved in the study
☒	☐ ChIP-seq
☒	☐ Flow cytometry
☒	☐ MRI-based neuroimaging

Clinical data

Policy information about clinical studies

All manuscripts should comply with the ICMJE guidelines for publication of clinical research and a completed CONSORT checklist must be included with all submissions.

Clinical trial registration	NCT03392428, ACTRN12615000912583
Study protocol	Trial details have been previously published in detail and are cited in Methods.
Data collection	Sample collection and initial processing details are available in the Supplementary Information. Information regarding patient recruitment to the original TheraP trial - including participating locations and enrollment timelines - have been published previously (NCT03392428; Hofman et al., Lancet 2021; Hofman et al., Lancet Oncology 2024).
Outcomes	Clinical endpoints evaluated in this study included PSA response rate, progression-free survival, and overall survival; extended definitions for these endpoints have previously been described and is cited in the Methods. PSA response rate was defined as the proportion of participants with a PSA reduction of ≥50% from baseline. Progression-free survival is defined as the interval from the date of randomisation to the date of first evidence of PSA progression (as per PCWG3 criteria), pain progression, radiographic progression, or death from any cause, whichever occurs first, or the date of last known follow-up without progression. Overall survival is defined as the interval from the date of registration to date of death from any cause, or the date of last known follow-up alive.

Plants

Seed stocks	*Report on the source of all seed stocks or other plant material used. If applicable, state the seed stock centre and catalogue number. If plant specimens were collected from the field, describe the collection location, date and sampling procedures.*
Novel plant genotypes	*Describe the methods by which all novel plant genotypes were produced. This includes those generated by transgenic approaches, gene editing, chemical/radiation-based mutagenesis and hybridization. For transgenic lines, describe the transformation method, the number of independent lines analyzed and the generation upon which experiments were performed. For gene-edited lines, describe the editor used, the endogenous sequence targeted for editing, the targeting guide RNA sequence (if applicable) and how the editor was applied.*
Authentication	*Describe any authentication procedures for each seed stock used or novel genotype generated. Describe any experiments used to assess the effect of a mutation and, where applicable, how potential secondary effects (e.g. second site T-DNA insertions, mosiacism, off-target gene editing) were examined.*